IET Generation, Transmission & Distribution

WILEY

The Institution of Engineering and Technology

ORIGINAL RESEARCH OPEN ACCESS

A New Algorithm for Multi-Objective Hybrid Economic Emission Dispatch Using Data-Driven Forecasting of Wind and Solar Power

Muhammad Kamran Khan[1] | Muhammad Ammar Khan[2] | Kimmo Kauhaniemi[1] | Muhammad Hamza Zafar[3] | Saad Rashid[2]

[1]School of Technology and Innovations, University of Vaasa, Vaasa, Finland | [2]Department of Electrical Engineering, Hamdard University, Islamabad, Pakistan | [3]Department of Engineering Sciences, University of Agder, Grimstad, Norway

Correspondence: Muhammad Kamran Khan (kamran.khan@uwasa.fi)

Received: 15 August 2025 | **Revised:** 20 October 2025 | **Accepted:** 3 November 2025

ABSTRACT

This study introduces a forecasting-driven framework for solving the hybrid dynamic economic emission dispatch (HDEED) problem with uncertain wind and solar generation. Unlike conventional approaches that rely on probabilistic models, this research uses data-driven forecasting techniques to predict the output powers of wind and PV plants and uses them in the multi-objective optimisation algorithm to minimise costs and emissions. An arithmetic optimiser with a sine cosine assisted driving training-based optimisation algorithm (AOASC-DTBO) is presented to solve various single and multi-objective HDEED problems based on fuzzy decision-making and the Pareto dominance concept. The proposed dispatching algorithm is validated using 10-unit, 40-unit and 7-unit IEEE 57 bus systems. The results revealed that the AOASC-DTBO algorithm achieved 8.73% and 4.95% lower fuel costs when compared with the PSO and DTBO algorithms, respectively. In addition, the emissions were 6.47% and 2.25% lower than the BMO and DTBO algorithms, respectively. The work highlights the importance of integrating renewable energy sources (RES) into power systems to achieve cost savings and reduced emissions, while also emphasising the need for efficient dispatch algorithms to ensure grid stability and reliability. The results demonstrate that integrating RES into the power system can yield substantial economic and environmental benefits, achieving cost savings of up to $6,908.034 and reducing emissions by 13,233.691 tonnes per day.

1 | Introduction

Economic load dispatch (ELD) can be classified into three main types. The first is static ELD, which optimises thermal unit power outputs to minimise fuel costs for a specified load and time period. The second is dynamic economic emission dispatch (DEED), an optimisation problem that simultaneously considers both cost and emission objectives while scheduling power generation from various sources to meet varying load demands over a 24 h horizon. The third type, hybrid dynamic economic emission dispatch (HDEED), extends DEED by incorporating both thermal and renewable energy sources (RES) [1]. HDEED determines the optimal combination of power generation from different sources such as coal-fired plants, gas-fired plants and renewables, while accounting for environmental impacts due to emissions. HDEED provides greater efficiency than conventional economic dispatch methods, making the approach particularly relevant in the current era characterised by high renewable energy penetration and growing environmental concerns.

There are two main categories of optimisation techniques used to solve the HDEED problem: classical and metaheuristic (MH)

approaches. Classical optimisation techniques, such as mixed integer quadratic programming (MIQP) [2], the fast λ-iteration method [3] and the interior point method [4], have been extensively applied to the economic dispatch problem. Although classical methods are computationally efficient, they face challenges when handling non-convex cost functions, particularly those affected by the valve-point effect (VPE). The VPE introduces ripples and makes cost curves non-smooth and discontinuous, which traditional methods struggle to handle effectively, often leading to suboptimal results [5, 6].

Consequently, metaheuristic optimisation techniques have gained prominence as robust alternatives for solving HDEED problems. These algorithms have demonstrated strong performance in practical applications, even when the mathematical properties of the cost function are complex. Over the past few decades, numerous MH algorithms have been successfully applied to DEED problems [7–11]. Examples include the arithmetic optimisation algorithm with three-dimensional chaotic mapping [12], the butterfly optimisation algorithm [13], the enhanced social network search algorithm [14], the enhanced zebra optimisation algorithm [15], the chaotic self-adaptive differential harmony search algorithm (CSADHS) [16], the improved tunicate swarm algorithm (ITSA) [17], the modulated particle swarm optimisation (MPSO) [18], the improved slime mould algorithm (ISMA) [19], enhanced differential evolution (EDE) [20], the chaotic artificial ecosystem-based optimisation algorithm (CAEO) [21], the hybrid harmony search algorithm (HHSA) [22], the whale optimisation algorithm (WOA) [23] and the improved bacterial foraging algorithm (IBFA) [24].

In recent years, researchers have focused on multi-objective approaches to address the DEED problem, incorporating both economic and environmental objectives alongside other system constraints such as power balance, ramping constraints and transmission losses [25–30]. Several multi-objective algorithms have been proposed, such as teaching-learning-based optimisation [31], hybrid multi-objective artificial gorilla troops optimiser [32], arithmetic optimisation algorithm with random searching strategies [33], non-dominated sorting multi-objective PSO [34], improved bare-bone multi-objective particle swarm optimisation (IBBMO-PSO) [35], multi-objective multi-verse optimisation (MOMV) [36], fast non-dominated time-varying acceleration coefficient-particle swarm optimisation (TVAC-PSO) [37], backtracking search algorithm (BSA) [38], modified marine predators algorithm (MMPA) [39], multi-objective membrane search algorithm (MOMSA) [40] and exchange market algorithm (EMA) [41].

Furthermore, the HDEED problem has gained significant attention in recent years due to the increasing penetration of RES in power systems [42, 43]. The uncertain and variable nature of renewable energy resources increases the complexity of the dispatch problem [44, 45]. In [1], an enhanced moth-flame optimisation (MFO) was used to solve HDEED problems. However, this study did not consider the impact of uncertain wind and solar power on the cost function. In [46], an improved mayfly algorithm (IMA) was applied to solve the HDEED problem, effectively optimising both economic and environmental objectives simultaneously. The results demonstrated the algorithm's superiority in terms of convergence and diversity compared to other methods. In [47], the authors proposed a stochastic dynamic ELD model that considers RES integration. To optimise economic dispatch, an improved fireworks algorithm (IFWA) with a non-uniform operator was utilised. The stochastic variability of wind and solar energy was modelled using Weibull and beta distributions, respectively. In [28], an improved sailfish optimisation (ISFO) algorithm was proposed to enhance solution quality and convergence speed for the HDEED problem, with the randomness of wind energy modelled using the Weibull distribution. In [42], the authors presented an HDEED model for a distributed power system, which included wind farms, thermal generating units and solar plants. An enhanced coot optimisation (COOT) algorithm, featuring a chaotic initialisation strategy, was proposed to improve both convergence performance and solution speed.

The literature review reveals that earlier HDEED studies predominantly employed probabilistic models to assess the dynamic impact of uncertainty in wind and PV power generation on the cost function. However, unlike conventional HDEED approaches that rely on probabilistic models, this study employs a data-driven forecasting framework to accurately predict the output power of wind and PV plants. These forecasts are directly integrated into a multi-objective HDEED formulation to jointly optimise generation scheduling, cost and emissions. To capture the dynamic impact of renewable uncertainty on operational costs, the model incorporates overestimation and underestimation penalties, which are applied when the available renewable power deviates from the scheduled output. This combined approach enables the production of clear, directly implementable generation schedules that are both economically optimal and operationally robust for real-time power system applications. The graphical abstract of the proposed model is given in Figure 1. The key contributions are:

- A forecasting-driven framework for solving the HDEED problem with uncertain wind and solar generation is proposed. The forecasted renewable energy data is effectively integrated into a multi-objective HDEED optimisation framework to determine optimal generation schedules, aiming to minimise both operational costs and environmental emissions.
- A novel arithmetic optimiser with sine cosine assisted driving training-based optimisation algorithm (AOASC-DTBO) algorithm is proposed that combines the strengths of the arithmetic optimisation and sine cosine algorithm (SCA) with the driving training-based optimisation (DTBO) algorithm. The proposed AOASC-DTBO is employed to address both single and multi-objective HDEED problems. For the multi-objective case, a fuzzy decision-making approach combined with the concept of Pareto dominance is integrated into the multi-objective AOASC-DTBO framework.
- An evolutionary neural network is proposed, in which the AOASC-DTBO algorithm optimises the hyperparameters of a radial basis function neural network (RBFNN) to give highly accurate short-term forecasts of wind and solar power generation.

The paper is divided into six sections. Section 2 presents multi-objective HDEED problem formulation, including the cost and emissions functions with their constraints. Section 3

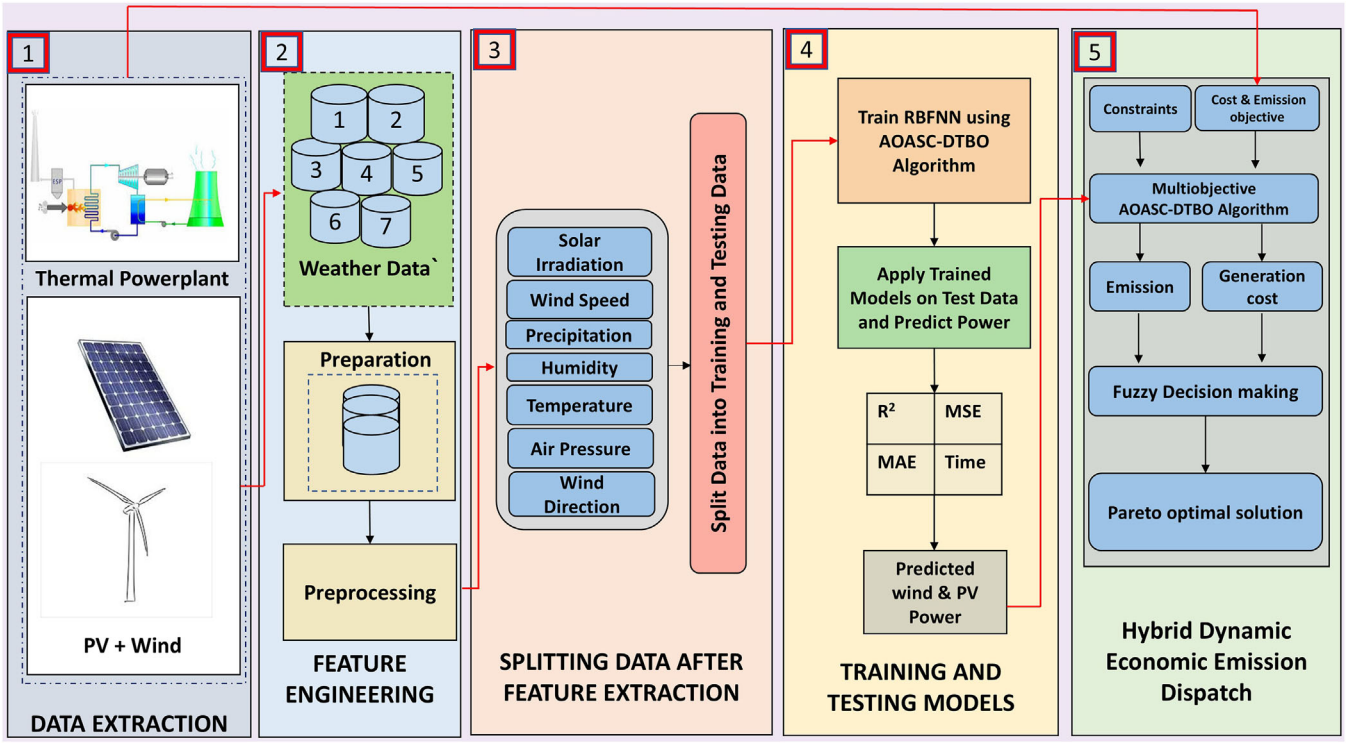

FIGURE 1 | Graphical demonstration of optimisation procedures and the utilised AOASC-DTBO algorithm in the multi-objective HDEED problem.

introduces the conventional DTBO and proposes the AOASC-DTBO algorithm. Evolutionary neural network-based based wind and photovoltaic (PV) power forecasting is presented in Section 4 while results and discussions are presented in Sections 5 and 6. Finally, Section 7 concludes the research.

2 | Formulation of Multi-Objective HDEED

The objective is to identify the optimal generation schedule that minimises both operational costs and environmental emissions. The problem formulation is organised into four subsections. Section 2.1 outlines the first objective, cost minimisation, while Section 2.2 presents the mathematical model for the second objective, emission minimisation. Section 2.3 details the mathematical formulation of the constraints and constraint handling mechanism, and Section 2.4 integrates these components to present the complete multi-objective HDEED model.

2.1 | Hybrid Dynamic Cost Objectives

The hybrid dynamic cost function is formulated as follows:

$$min\ F_c = \sum_{t=1}^{h}\left(\sum_{i=1}^{NG} F_c\left(P_{Gi,t}\right) + \sum_{j=1}^{NS} F_c\left(P_{pvj,t}\right) + \sum_{k=1}^{NW} F_c\left(P_{wk,t}\right)\right) \tag{1}$$

where F_c is fuel cost and t is time horizon. NG is the number of thermal units, NS and NW are the number of PV and wind units, respectively. Similarly, P_G, P_{pv} and P_{wk} and represent thermal, PV and wind power generation and $F_c(P_{Gi,t})$, $F_c(P_{pvj,t})$, $F_c(P_{wk,t})$ represent fuel cost of thermal and wind generation. The fuel cost of thermal generation is formulated as a non-convex function.

$$F_c\left(P_{Gi,t}\right) = \sum_{i=1}^{NG}\left(a_i + b_i P_{Gi,t} + c_i P_{Gi,t}^2 + \left|d_i \sin\left\{e_i\left(P_{Gi,t}^{min} - P_{Gi,t}\right)\right\}\right|\right) \tag{2}$$

Where a_i, b_i, c_i, d_i and e_i represent cost coefficients. P_G represents thermal power generation and NG is the number of thermal units. The sine function is included to model the valve point effect in thermal units. The second term of Equation (1), $F_c(P_{pvj,t})$, represents the operating cost of solar generation and can be modelled as:

$$F_c\left(P_{pvj,t}\right) = \sum_{j=1}^{NS} F_{pvj}\left(P_{pvj,t}\right) + \sum_{j=1}^{NS} F_{U,pvj}\left(P_{pvj,act,t} - P_{pvj,t}\right) + \sum_{j=1}^{NS} F_{O,pvj}\left(P_{pvj,t} - P_{pvj,act,t}\right) \tag{3}$$

The first part of Equation (3) is the direct cost of solar power generation, which reflects the cost of producing energy from the PV. This cost is proportional to the power generated by the PV system and is calculated as the product of the scheduled PV power at time t and the cost coefficient $k_{dc,pvj}$.

$$F_{pvj}\left(P_{pvj,t}\right) = k_{dc,pvj} * P_{pvj,t} \tag{4}$$

The second and third terms of Equation (3) model the effects of under- and over-utilisation of PV power on the cost function. The second term represents the underestimation penalty cost incurred

by the power system operator when available solar power is not fully utilised, as modelled in Equation (5):

$$F_{U,pvj} = k_{up,pvj} * \left(P_{pvj,act,t} - P_{pvj,t}\right) \tag{5}$$

where $P_{pvj,act,t}$ is the actual solar power at time t, $P_{pvj,t}$ is the scheduled solar power at time t, and k_{up} is the underestimation penalty coefficient. The third part of (3) is the overestimation reserve cost, which models the scenario when the available solar power is lower than the scheduled solar power, as given in Equation (6):

$$F_{O,pvj} = k_{op,pvj} * \left(P_{pvj,t} - P_{pvj,act,t}\right) \tag{6}$$

where k_{op} is the overestimation penalty coefficient. The third term of Equation (1), $F_c(P_{wk,t})$, represents the operating cost of wind power generation and can be modelled in a similar way as the operating cost of PV is modelled.

$$F_c\left(P_{wk,t}\right) = \sum_{k=1}^{NW} F_{wk}\left(P_{wk,t}\right) + \sum_{k=1}^{NW} F_{U,wk}\left(P_{wk,act,t} - P_{wk,t}\right) + \sum_{k=1}^{NW} F_{O,wk}\left(P_{wk,t} - P_{wk,act,t}\right) \tag{7}$$

The first part of Equation (7) is the direct cost of wind power generation. This cost is proportional to the power generated by the wind and is calculated as the product of the scheduled wind power at time t ($P_{wk,t}$) and the cost coefficient $k_{dc,wk}$.

$$F_{wk}\left(P_{wk,t}\right) = k_{dc,wk} * P_{wk,t} \tag{8}$$

The second term of the Equation (7) is underestimation penalty for wind generation as modelled in Equation (9):

$$F_{U,wk} = k_{up,wk} * \left(P_{wk,act,t} - P_{wk,t}\right) \tag{9}$$

where $P_{wk,act,t}$ is the actual wind power at time t, $P_{wk,t}$ is the scheduled wind power at time t and k_{up} is the underestimation penalty coefficient. The third term of the Equation (7) is the overestimation reserve cost for wind generation and is expressed as:

$$F_{O,wk} = k_{op,wk} * \left(P_{wk,t} - P_{wk,act,t}\right) \tag{10}$$

2.2 | Hybrid Dynamic Emission Objectives

The emission function of atmospheric pollutants from thermal units is expressed by Equation (11):

$$min\ E_c = \sum_{t=1}^{h}\left(\sum_{i=1}^{NG}\left(\alpha_i + \beta_i P_{Gi,t} + \gamma_i P_{Gi,t}^2 + \zeta_i \exp\left(\delta_i P_{Gi,t}\right)\right) + E_{O,wi} + E_{O,pvi}\right) \tag{11}$$

where α_i, β_i, γ, ζ_i and δ_i are emission coefficients of the ith unit. E_c is the total emission. The terms $E_{O,wi}$ and $E_{O,pvi}$ modelled the effect of over utilisation of wind and PV capacity in the emission cost function. The overestimation reserve cost for wind emission is given by:

$$E_{O,wi} = e_{op,wi} * \left(P_{wi,t} - P_{wi,act,t}\right) \tag{12}$$

where $P_{wi,act,t}$ is the actual wind power at time t, $P_{wi,t}$ is the scheduled wind power at time t and $e_{op,wi}$ is the overestimation emission penalty coefficient. The overestimation reserve cost for PV emission is:

$$E_{O,pvi} = e_{op,pvi} * \left(P_{pvi,t} - P_{pvi,act,t}\right) \tag{13}$$

where $P_{pvi,act,t}$ is the actual solar power at time t, $P_{pvi,t}$ is the scheduled PV power at time t and $e_{op,pvi}$ is the overestimation emission penalty coefficient.

2.3 | Constraints for HDEED

In this subsection, we discuss the major constraints of the HDEED problem and the penalty-function-based mechanism used to handle constraint violations.

2.3.1 | Power Balance Constraints

Under all conditions, the total generation from thermal, PV and wind sources must equal the total load demand, including transmission losses.

$$\sum_{i=1}^{NG} P_{Gi,t} + \sum_{j=1}^{NS} P_{pvj,t} + \sum_{k=1}^{NW} P_{wk,t} = P_{d,t} + P_{loss,t} \tag{14}$$

Where $P_{d,t}$ is the load demand and $P_{loss,t}$ is power losses.

$$P_{loss_t} = \sum_{i=1}^{N}\sum_{j=1}^{N}\left(P_{Gi,t} B_{ij} P_{Gj,t}\right) + \sum_{j=1}^{N}\left(B_{0i} P_{Gi,t}\right) + B_{00} \tag{15}$$

Where B_{ij}, B_{0i} and B_{00} are the transmission loss coefficients.

2.3.2 | Real Power Inequality Constraint

The real power constraints for thermal, PV and wind power plants are given in Equations (16)–(18), respectively.

$$P_{Gi,t}^{min} \le P_{Gi,t} \le P_{Gi,t}^{max} \tag{16}$$

$$P_{pvj,t}^{min} \le P_{pvj,t} \le P_{pvj,t}^{max} \tag{17}$$

$$P_{wk,t}^{min} \le P_{wk,t} \le P_{wk,t}^{max} \tag{18}$$

2.3.3 | Ramp Rate Limits

The constraints for ramp rate are:

$$P_{Gi,t} - P_{Gi,t-1} \le UR_i \tag{19}$$

$$P_{Gi,t-1} - P_{Gi,t} \le DR_i \tag{20}$$

$$\max\left(P_{Gi}^{min}, P_{Gi,t-1} - DR_i\right) \le P_{Gi,t} \le \min\left(P_{Gi}^{max}, P_{Gi,t-1} + UR_i\right) \tag{21}$$

where UR_i is the ramp upper limit and DR_i is the ramp down limit of the ith thermal unit.

2.3.4 | Penalty Function-Based Constraint Handling Mechanism

In this study, the penalty function method is utilised to handle power balance constraints defined in Equation (14). The mechanism converts a constrained multi-objective HDEED problem into an unconstrained problem using a penalty factor. The procedure is explained below:

Step1: Compute transmission losses using Equation (15)
Step 2: Compute fuel cost using Equation (1). The cost function includes thermal, wind and PV generation cost.
Step 3: Compute emission cost using Equation (11).
Step 4: Check power balance constraints using Equation (14).
Step 5: Handle the constraint violation using a penalty factor as defined below:

$$\lambda = max\left(0, 1 - \frac{\sum_i P_i - P_{loss}}{P_d}\right) \tag{22}$$

where P_i and P_d are the scheduled and demanded powers at time t.
Step 6: Apply the penalty to the multi-objective cost function vector $[F_c, E_c]$.

$$F_p = [F_c, E_c].(1 + k\lambda) \tag{23}$$

By choosing a large value of k (i.e., 1000), the mechanism ensures that infeasible solutions (those violating demand balance) are assigned much higher objective values, guiding the optimisation algorithm toward feasible and efficient dispatch solutions.

2.4 | Multi-Objective HDEED Objective Function

The bi-objective optimisation problem for HDEED involves minimising the two conflicting objectives, fuel cost (F_c) defined in Section 2.1 and emission (E_c) defined in Section 2.2, subjected to the constraints defined in Section 2.3. The mathematical representation of this multi-objective optimisation problem is as follows:

$$\begin{cases} min\ F = [F_c, E_c] \\ subject\ to\ constraints\ defined\ in\ 2.3.1, 2.3.2, 2.3.3 \end{cases} \tag{24}$$

Here, $\boldsymbol{F}$ represents the multi-objective cost function, which integrates both the fuel cost minimisation objective ($\boldsymbol{F}_c$) defined in Equation (1) and the emission minimisation objective ($\boldsymbol{E}_c$) defined in Equation (11). The paper proposes a multi-objective optimisation approach for power systems, with two objective functions: minimising fuel cost and minimising emissions. The problem is subjected to constraints defined in Section 2.3. If these constraints are violated, the cost function is penalised. The optimisation algorithm identifies both dominated and non-dominated solutions based on Pareto dominance and stores the non-dominated ones in an archiving matrix. The best compromise solution (BCS) is then determined from the non-dominated solutions using the fuzzy decision making (FDM) method.

3 | AOASC-DTBO for HDEED

3.1 | Conventional Driving Training-Based Optimisation (DTBO)

DTBO is a metaheuristic technique that relies on a population-based approach, and its members are comprised of driving learners and instructors [48]. In the initialisation phase population matrix is defined as shown in (25) and (26):

$$X = \begin{bmatrix} X_1 \\ \vdots \\ X_i \\ \vdots \\ X_P \end{bmatrix}_{P\times z} = \begin{bmatrix} x_{11} & \dots & x_{1j} & \dots & x_{1z} \\ \vdots & \ddots & \vdots & \ddots & \vdots \\ x_{i1} & \dots & x_{ij} & \dots & x_{iz} \\ \vdots & \ddots & \vdots & \ddots & \vdots \\ x_{P1} & \dots & x_{Pj} & \dots & x_{Pz} \end{bmatrix}_{P\times z} \tag{25}$$

$$\begin{aligned} x_{i,j} &= x_{min,j} + r \times \left(x_{max,j} - x_{min,j}\right) \\ i &= 1, 2, \dots, P \quad j = 1, 2 \dots, z \end{aligned} \tag{26}$$

where $x_{i,j}$ position of ith candidate solution in jth dimension, P is the population size and z represent dimensions of the problem, r is random number in range [0,1] while x_{min} and x_{max} represents lower and upper bounds. The objective function is modelled using a vector F in (27):

$$F = \begin{bmatrix} F_1 \\ \vdots \\ F_i \\ \vdots \\ F_P \end{bmatrix}_{P\times 1} = \begin{bmatrix} F(X_1) \\ \vdots \\ F(X_i) \\ \vdots \\ F(X_P) \end{bmatrix}_{P\times 1} \tag{27}$$

The method used to update candidate solutions is what distinguishes MH algorithms from one another. Candidate solutions in DTBO are updated during the three stages as follows: (1) teaching by a driving instructor, (2) modelling learner-driver behaviour after instructor behaviours and (3) practising by the learner-driver.

3.1.1 | Teaching by a Driving Instructor

This stage of the DTBO illustrates this algorithm's exploratory capabilities. In each iteration P members are selected as driving instructors using (28):

$$D = \begin{bmatrix} D_1 \\ \vdots \\ D_i \\ \vdots \\ D_{P_D} \end{bmatrix}_{P_D\times z} = \begin{bmatrix} D_{11} & \dots & D_{1j} & \dots & D_{1z} \\ \vdots & \ddots & \vdots & \ddots & \vdots \\ D_{i1} & \dots & D_{ij} & \dots & D_{iz} \\ \vdots & \ddots & \vdots & \ddots & \vdots \\ D_{P_D1} & \dots & D_{P_Dj} & \dots & D_{P_Dz} \end{bmatrix}_{P_D\times z} \tag{28}$$

$$P_D = \left[0.1 * P * \left(1 - \frac{t}{T}\right)\right] \tag{29}$$

where D = driving instructor matrix, P_D is the number of driving instructors, t is the iteration counter and T is the maximum number of iterations. To mathematically describe the DTBO phase, the new location of each member is first determined using Equation (30). If the new location (X_i^{p1}) improves the value of the objective function (F_i^{p1}), the previous location (X_i) will be replaced, as specified by Equation (31).

$$x_{i,j}^{P1} = \begin{cases} x_{i,j} + d \cdot \left(D_{k_{i,j}} - I \cdot x_{i,j}\right), & F_{DI_{k_i}} < F_i \\ x_{i,j} + d \cdot \left(x_{i,j} - D_{k_i,j}\right), & \text{otherwise} \end{cases} \tag{30}$$

$$X_i = \begin{cases} X_i^{p1}, & F_i^{p1} < F_i \\ X_i, & \text{otherwise} \end{cases} \tag{31}$$

where I is a number randomly chosen from the set {1, 2} [12], d is a random number chosen from the range [0, 1], X_i^{p1} is the new calculated status for the ith candidate solution based on the first phase of DTBO, $x_{i,j}^{P1}$ is its jth dimension, F_i^{p1} is its objective function value, D_{k_i}, where k_i is randomly selected from the range [1, 2,..., P_D], represents a selected driving instructor and $D_{k_{i,j}}$ is the jth dimension.

3.1.2 | Modelling Learner Driver Behaviour

In this stage a position is updated based on the linear combination of each member with the teacher in accordance with Equation (32). If the objective function improves, the new location will replace the previous ones.

$$x_{i,j}^{P2} = P \cdot x_{i,j} + (1 - P) \cdot D_{k_i,j} \tag{32}$$

$$X_i = \begin{cases} X_i^{p2}, & F_i^{p2} < F_i \\ X_i, & \text{otherwise} \end{cases} \tag{33}$$

where X_i^{p2} = the updated position based on the learner driver phase of DTBO, $x_{i,j}^{P2}$ = jth dimension, F_i^{p2} = cost function value and P = patterning index.

3.1.3 | Modelling Personal Practice

The personal practice phase of DTBO is described in Equation (34), where a random position is initially generated, close to each member of the population. If this position leads to an improvement in the value of the objective function, the previous position will be replaced, as specified in Equation (35).

$$x_{i,j}^{p_3} = x_{i,j} + (1 - 2d) \cdot S \cdot \left(1 - \frac{t}{T}\right) \cdot x_{i,j} \tag{34}$$

$$X_i = \begin{cases} X_i^{p3}, & F_i^{p3} < F_i \\ X_i, & \text{otherwise} \end{cases} \tag{35}$$

where d is random number from the range [0, 1], $S = 0.05$, t is the iteration counter, and T is the maximum number of iterations. X_i^{p3} is the new calculated status for the ith candidate solution based on the third phase of DTBO, $x_{i,j}^{p_3}$ is its jth dimension and F_i^{p3} is its objective function value.

3.2 | Proposed AOASC-DTBO Algorithm

In this work, the AOASC-DTBO algorithm is presented. DTBO is a recently developed optimisation algorithm. But while solving nonconvex optimisation problems like HDEED with many dimensions, DTBO may encounter slow convergence, high computational complexity, and the risk of getting stuck in local minima. As a solution, in this research, some modifications are given to the original DTBO algorithm to address these issues.

To prevent being trapped in a local minimum, the potential candidates must explore the feasible region extensively. To achieve this, the learner driver stage of the DTBO algorithm incorporates a sine cosine operator based on the mathematical concepts of the SCA [49]. By including the sine cosine operators, the DTBO algorithm gains global exploration capabilities that allow the algorithm to better explore the feasible space and find more promising regions to search, which can lead to improved optimisation performance. Therefore, the original Equations (32) and (33) in the DTBO algorithm are replaced with a new equation.

$$x_{i,j}^{P2} = \begin{cases} x_{i,j} + rand() \times \sin(rand()) \times \left| rand() \times best\left(d_j\right) - x_{i,j} \right|, \\ r_1 < 0.5 \\ x_{i,j} + rand() \times \cos(rand()) \times \left| rand() \times best\left(d_j\right) - x_{i,j} \right|, \\ r_1 \geq 0.5 \end{cases} \tag{36}$$

$$X_i = \begin{cases} X_i^{p2}, & F_i^{p2} < F_i \\ X_i, & \text{otherwise} \end{cases} \tag{37}$$

where $rand()$ and r_1 represent randomly chosen numbers between 0 and 1. The r_1 switches between sine and cosine functions. If r_1 is less than 0.5, the position is updated using *sin* function otherwise *cos* function is used. X_i^{p2} = updated position based on sine cosine operator, $x_{i,j}^{P2}$ = jth dimension and F_i^{p2}= cost function value. If the new position based on the sine cosine operator (X_i^{p2}) improves the value of the objective function (F_i^{p2}) the previous position (X_i) will be replaced.

Furthermore, the improved algorithm also incorporates a math optimisation probability (MOP) coefficient in the personal practice stage of DTBO to enhance exploitation. The MOP coefficient is inspired by the arithmetic optimisation algorithm (AOA) [50] and allows solution candidates to search the area closest to the current solution, thereby improving exploitation capabilities. Therefore, in the AOASC-DTBO algorithm, Equations (34) and (35) are replaced with a new equation:

$$x_{i,j}^{p_3} = x_{i,j} + (1 - 2d) \cdot S \cdot MOP \cdot x_{i,j} \tag{38}$$

$$X_i = \begin{cases} X_i^{p3}, & F_i^{p3} < F_i \\ X_i, & \text{otherwise} \end{cases} \tag{39}$$

$$MOP(t) = 1 - \frac{t^{1/alpha}}{T^{1/\alpha}} \tag{40}$$

where α is the sensitivity parameter, which defines the accuracy of the exploitation during the iterative process. t is the iteration counter and T is the maximum number of iterations. The

ALGORITHM 1 | AOASC-DTBO Pseudo-Code.

Initialize *random population p*
Initialize *counter t = 0 & max iteration T, α and S*
for *t = 1: T*
Evaluate fitness
for *i = 1: p*
First phase
Randomly select driving instructor D
Determine new position using (30)
Update position using (31)
Second phase
Determine new position using (36)
Update position using (37)
Third phase
Calculate MOP using (40)
Determine new position using (38)
Update position using (39)
end
Update best position
end
Return *best position*

pseudo-code of the proposed AOASC-DTBO is presented in Algorithm 1 below.

3.3 | Experimental Verification

In this section, the AOASC-DTBO is tested using standard benchmark unimodal and multimodal functions. To verify the effectiveness of the proposed algorithm, the results of AOASC-DTBO are compared with several other optimisation algorithms, including DTBO, grey wolf optimiser (GWO) [51], discrete firefly algorithm (DFA) [52], PSO, coyote optimisation algorithm (COA) [53] and arithmetic optimisation algorithm (AOA). The best, average and worst cost values and standard deviations achieved by various comparing algorithms in 1000 iterations with a population size of 30 are presented in Table 1. The results confirm the superior performance of AOASC-DTBO, which ranked first in 20 out of 21 test functions and achieved an overall rank of 1.047, significantly lower than the 1.428 rank of the DTBO algorithm. The convergence curves of some of the selected test functions are presented in Figure 2. The results show that the proposed AOASC-DTBO algorithm combines the strengths of the arithmetic optimisation and sine cosine algorithm with the DTBO algorithm to overcome limitations of DTBO and achieve better performance in solving nonconvex optimisation problems with high dimensions.

4 | Evolutionary Neural Network-Based Wind and PV Power Forecasting

While wind and solar are promising renewable sources, their output is highly dependent on stochastic weather conditions, which complicates their integration into the grid. Accurate energy prediction is essential for efficient generation scheduling, reliable operational planning and optimal market operations. To address this challenge, the proposed solution employs a RBFNN for short-term wind and solar power forecasting. The RBFNN maps the input data to a higher-dimensional space using radial basis functions in the hidden layer. This transformation enables the network to capture non-linear relationships and complex patterns in the data. The output layer then generates the predicted values based on the input data and the weights of the network, resulting in reliable and accurate forecasting. The expression for hidden layer neurone is presented in Equation (41):

$$\phi_j = e^{\left(-\frac{\left(||X-\bar{u}_j||^2\right)}{2*\zeta_j{}^2}\right)} \tag{41}$$

where X is the input vector, $\bar{u}_j$ is j^{th} neurone's vector, $\zeta_j = j^{\text{th}}$ neurone's bandwidth, $\phi_j = j^{\text{th}}$ neurone's output. The output layer of an RBFNN performs different linear computations which can be represented mathematically as:

$$Y = \sum_{k}^{n} \mathrm{w}_k \phi_k \tag{42}$$

where w_k is the weight connection, ϕ_k is jth neurone's output and Y is the prediction result. The RBFNN is presented in Figure 3.

4.1 | Training Neural Network Using AOASC-DTBO Algorithm

Classification and prediction accuracy can be enhanced by optimally tuning the RBFNN hyperparameters, such as the weights and the smoothing parameter (σ). Traditionally, gradient-based methods are employed to train neural networks, but these methods are usually sensitive to the initial conditions and often get trapped in local minima, which may result in degraded performance [54]. To overcome these challenges and minimise prediction errors, the AOASC-DTBO algorithm is utilised to determine the weight and σ parameters. The flowchart for the proposed evolutionary RBFNN is presented in Figure 4.

The initial step in the forecasting process is to prepare the dataset, which includes selecting the appropriate input and output features. For solar power forecasting, the input features typically include ambient temperature, module temperature and irradiance, while the output feature is the AC power. In contrast, for wind power forecasting, the input features include wind speed and direction, and the output feature is wind power generation. To train the neural network, approximately 80% of the data is used for training, and the remaining 20% is used for validation. The neural network is initialised with a single hidden layer, and the number of neurones in this layer is determined using a random process. In this work, the number of neurones is determined by using (43):

$$N = 2 \times C + 1 \tag{43}$$

where C is the number of input features and N is the number of selected neurons.

The algorithm starts by initialising the RBFNN with random weights and biases and then initialising the AOASC-DTBO algorithm with random population size, stopping criteria and other parameters. The algorithm then updates the weights and bias of

TABLE 1 | Statistical results (best, worst, average, STD) of various algorithms on standard benchmark functions.

Fun.	Params	AOASC-DTBO	DTBO	COA	AOA	BMO	DFA	PSO
F1	Best	**0**	**0**	**0**	0	2.53×10^{-41}	1.71×10^{-241}	6.332×10^{-5}
	Worst	**0**	**0**	**0**	0	8.1987×10^{-17}	3.2422×10^{3}	3.8626×10^{1}
	Avg	**0**	**0**	**0**	0	2.7539×10^{-18}	1.4563×10^{-3}	3.0172×10^{1}
	Std	**0**	**0**	**0**	0	1.4965×10^{-17}	6.5066×10^{2}	1.0142×10^{1}
	Rank	**1**	**1**	**1**	1	2	3	4
F2	Best	**0**	**0**	**0**	1.0×10^{-113}	4.96×10^{-14}	2.00×10^{-2}	0.46662
	Worst	**0**	**0**	**0**	5.3×10^{-109}	7.0783×10^{-11}	6.0004×10^{1}	4.3965
	Avg	**0**	**0**	**0**	4.7×10^{-110}	8.3466×10^{-12}	2.4167×10^{1}	2.9880
	Std	**0**	**0**	**0**	1.04×10^{-10}	1.6779×10^{-11}	1.0223×10^{1}	1.0121
	Rank	**1**	**1**	**1**	2	3	4	5
F3	Best	**0**	**0**	**0**	1.77×10^{-60}	6.58×10^{-20}	179.72	279.44
	Worst	**0**	**0**	**0**	3.6307×10^{-2}	9.9208×10^{-3}	1.3762×10^{4}	1.3666×10^{3}
	Avg	**0**	**0**	**0**	2.4297×10^{-3}	3.3073×10^{-4}	5.6410×10^{3}	1.0504×10^{3}
	Std	**0**	**0**	**0**	7.7154×10^{-3}	1.8113×10^{-3}	3.4737×10^{3}	2.7036×10^{2}
	Rank	**1**	**1**	**1**	2	3	4	5
F4	Best	**0**	**0**	**0**	9.2×10^{-101}	1.24×10^{-12}	11.9265	22.2906
	Worst	**0**	**0**	**0**	4.7766×10^{-2}	3.2585×10^{-7}	3.3973×10^{1}	28.6627
	Avg	**0**	**0**	**0**	1.8316×10^{-62}	1.7258×10^{-8}	2.2926×10^{1}	24.6804
	Std	**0**	**0**	**0**	2.1226×10^{-9}	6.6769×10^{-8}	4.0363×10	6.0177×10^{-1}
	Rank	**1**	**1**	**1**	2	3	4	5
F5	Best	**0**	**0**	**0**	5.43×10^{-43}	8.973	11.458	32.031
	Worst	**0**	**0**	**0**	2.8762×10^{1}	2.9000×10^{1}	1.7465×10^{6}	9.6222×10^{2}
	Avg	**0**	**0**	**0**	2.8226×10^{-21}	2.8993×10^{1}	3.9378×10^{5}	7.2410×10^{2}
	Std	**0**	**0**	**0**	3.8094×10^{-1}	8.2050×10^{-3}	3.7538×10^{5}	2.5981×10^{2}
	Rank	**1**	**1**	**1**	2	3	4	5
F6	Best	**0**	**0**	**0**	3.23×10^{-10}	7.0944	1.70×10^{3}	37.6957
	Worst	**0**	**0**	**0**	3.1201×10	7.5000	3.1583×10^{3}	3.4095×10^{1}
	Avg	**0**	**0**	**0**	2.6864×10^{-4}	7.2586	1.6669×10^{3}	2.6349×10^{1}
	Std	**0**	**0**	**0**	2.7143×10^{-1}	2.5451×10^{-1}	5.3343×10^{2}	5.7192×10
	Rank	**1**	**1**	**1**	2	3	5	4
F7	Best	$\mathbf{1.07 \times 10^{-7}}$	1.24×10^{-6}	1.47×10^{-5}	7.79×10^{-5}	0.0474	0.3329	0.0453
	Worst	$\mathbf{1.79 \times 10^{-4}}$	5.9204×10^{-5}	9.9393×10^{-5}	1.9551×10^{-5}	5.4937×10^{-2}	1.5916×10	7.1927×10^{-2}
	Avg	$\mathbf{3.61 \times 10^{-5}}$	4.0435×10^{-5}	4.5069×10^{-5}	2.3949×10^{-5}	1.4400×10^{-2}	7.5192×10^{-1}	4.7281×10^{-2}
	Std	$\mathbf{3.37 \times 10^{-5}}$	1.5547×10^{-5}	2.5525×10^{-5}	2.7019×10^{-5}	1.3560×10^{-2}	3.6078×10^{-1}	1.6643×10^{-2}
	Rank	**1**	2	3	4	5	5	6
F8	Best	$\mathbf{-1.29 \times 10^{4}}$	−12569.5	−12515.2	−6068.2	−3376.7	−5654.8	−4992.3
	Worst	$\mathbf{-9.01 \times 10^{3}}$	-9.02×10^{3}	−8569.1	−5075.3	-1.8853×10^{3}	-2.2373×10^{3}	-4.995×10^{3}
	Avg	$\mathbf{-1.15 \times 10^{4}}$	-1.17×10^{4}	−10569.7	−57928.1	-2.7712×10^{3}	-4.0865×10^{3}	-5.811×10^{3}
	Std	$\mathbf{1.65 \times 10^{3}}$	1.71×10^{3}	4.2641×10^{3}	3.3942×10^{2}	5.4369×10^{2}	1.2683×10^{3}	6.0527×10^{2}
	Rank	**1**	2	3	4	5	6	7

(Continues)

TABLE 1 | (Continued)

Fun.	Params	AOASC-DTBO	DTBO	COA	AOA	BMO	DFA	PSO
F9	Best	**0**	**0**	**0**	**0**	**0**	146.1292	41.0019
	Worst	**0**	**0**	**0**	**0**	**0**	1.8550×10^{2}	5.5204×10^{1}
	Avg	**0**	**0**	**0**	**0**	**0**	1.4594×10^{2}	4.6123×10^{1}
	Std	**0**	**0**	**0**	**0**	**0**	2.2610×10^{1}	5.8122×10
	Rank	**1**	**1**	**1**	**1**	**1**	3	2
F10	Best	$\mathbf{1.22 \times 10^{-16}}$	8.87×10^{-16}	8.88×10^{-16}	9.18×10^{-16}	5.1671×10^{-10}	19.9657	3.5598
	Worst	$\mathbf{1.22 \times 10^{-16}}$	8.87×10^{-16}	8.88×10^{-16}	9.18×10^{-16}	1.0090×10^{-9}	1.9967×10^{1}	3.7816×10
	Avg	$\mathbf{1.22 \times 10^{-16}}$	8.87×10^{-16}	8.88×10^{-16}	9.18×10^{-16}	7.3623×10^{-9}	1.9121×10^{1}	3.1344×10
	Std	**0**	0	0	0	2.1625×10^{-10}	2.6057×10	5.0092×10^{-1}
	Rank	**1**	2	3	4	5	6	7
F11	Best	**0**	**0**	**0**	0.1077	0	13.8931	1.2018
	Worst	**0**	**0**	**0**	0.3087	0	3.8131×10^{1}	1.3894×10
	Avg	**0**	**0**	**0**	0.1235	0	1.5438×10^{1}	1.2461×10
	Std	**0**	**0**	**0**	7.4923×10^{-2}	0	6.5036×10	9.2251×10^{-2}
	Rank	**1**	**1**	**1**	2	1	4	3
F12	Best	$\mathbf{0.87 \times 10^{-32}}$	1.56×10^{-32}	1.66×10^{-32}	0.3959	1.6202	0.5714	7.6596
	Worst	$\mathbf{1.00 \times 10^{-12}}$	2.3576×10^{-10}	1.66×10^{-9}	0.4738	1.6688	4.7415×10^{5}	9.5694×10
	Avg	$\mathbf{5.97 \times 10^{-14}}$	1.1101×10^{-11}	1.66×10^{-10}	0.41975	1.5111	1.6945×10^{4}	4.6205×10
	Std	$\mathbf{2.29 \times 10^{-13}}$	4.5199×10^{-11}	5.5674×10^{-10}	4.4454×10^{-2}	2.0113×10^{-1}	8.6498×10^{4}	3.1533×10
	Rank	**1**	2	3	4	5	6	7
F13	Best	$\mathbf{8.33 \times 10^{-33}}$	1.44×10^{-32}	1.54×10^{-32}	2.9383	2.9973	4.95×10^{3}	4.6894
	Worst	$\mathbf{2.76 \times 10^{-9}}$	2.8436×10^{-9}	1.54×10^{-8}	2.9415	3.0000	0.4577×10^{6}	4.9780×10
	Avg	$\mathbf{1.39 \times 10^{-10}}$	1.1232×10^{-10}	1.54×10^{-8}	2.9405	2.9993	1.9592×10^{5}	4.7285×10
	Std	$\mathbf{5.59 \times 10^{-11}}$	5.1894×10^{-10}	1.058×10^{-10}	9.2959×10^{-2}	9.2116×10^{-4}	3.6976×10^{5}	1.0379×10
	Rank	**1**	2	3	4	5	6	7
F14	Best	**0.8560**	0.9980	0.9980	1.6705	4.2021	1.9920	0.9980
	Worst	$\mathbf{6.90 \times 10}$	8.9821×10	0.9980	2.2671	1.2671×10^{1}	1.5504×10^{1}	2.9821×10
	Avg	$\mathbf{1.49 \times 10}$	1.634×10	0.9980	1.9979	7.6247	5.8990×10	1.4206×10
	Std	$\mathbf{1.50 \times 10}$	5.2656×10	0	4.4543×10	3.8501×10	3.8958×10	8.7468×10^{-1}
	Rank	**1**	2	3	4	5	6	7
F15	Best	$\mathbf{3.07 \times 10^{-4}}$	$\mathbf{3.07 \times 10^{-4}}$	3.85×10^{-4}	4.16×10^{-4}	0.0044	7.82×10^{-4}	0.0015
	Worst	$\mathbf{3.07 \times 10^{-4}}$	$\mathbf{3.07 \times 10^{-4}}$	6.1598×10^{-4}	1.0712×10^{-1}	9.9163×10^{-2}	2.0363×10^{-2}	7.0646×10^{-3}
	Avg	$\mathbf{3.07 \times 10^{-4}}$	$\mathbf{3.07 \times 10^{-4}}$	3.7704×10^{-4}	1.5400×10^{-2}	9.8613×10^{-3}	4.3868×10^{-3}	6.4573×10^{-4}
	Std	**0**	**0**	9.0936×10^{-5}	2.6599×10^{-2}	1.9379×10^{-2}	7.2054×10^{-3}	6.1702×10^{-5}
	Rank	**1**	**1**	2	3	5	4	6
F16	Best	**−1.0332**	−1.0316	−1.0171	−1.0141	−1.0227	−1.0162	−1.411
	Worst	**−1.0332**	−1.0316	−1.0171	−1.0141	-2.6604×10^{-1}	−1.0162	−1.411
	Avg	**−1.0332**	−1.0316	−1.0171	−1.0141	-9.3455×10^{-1}	−1.0162	−1.411
	Std	**0**	0	4.3571×10^{-5}	0	1.7469×10^{-1}	0	0
	Rank	**1**	2	3	4	6	5	7

(Continues)

TABLE 1 | (Continued)

Fun.	Params	AOASC-DTBO	DTBO	COA	AOA	BMO	DFA	PSO
F17	Best	**0.3865**	0.3979	0.3979	0.4128	0.4474	0.5664	0.6325
	Worst	**0.3865**	0.3978	0.4010	4.2075×10^{-1}	6.7328	8.1402	0.6325
	Avg	**0.3865**	0.3978	0.3984	4.1567×10^{-1}	9.3946×10^{-1}	5.3341	0.6325
	Std	**0**	5.3817×10^{-20}	8.7303×10^{-4}	6.2296×10^{-3}	1.2943	0.11657	0
	Rank	**1**	2	3	4	5	6	7
F18	Best	**2.94**	3	3.022	3	4.8106	3.0000	3.0000
	Worst	**3.00**	3.02	3.7943	9.7216×10^{1}	3.1587×10^{1}	3.0000	3.0000
	Avg	**2.98**	3.01	3.0837	1.1377×10^{1}	9.5346	3.0000	3.0000
	Std	$\mathbf{2.98 \times 10^{-11}}$	7.65×10^{-9}	1.6026×10^{-1}	1.9380×10^{1}	9.2683×10	0	0
	Rank	**1**	2	3	4	5	6	6
F19	Best	**−3.863**	−3.8627	−3.7824	−3.8573	−3.7436	−3.8620	−3.8620
	Worst	**−3.8613**	−3.8626	−3.3875	−3.8544	−3.2222	−3.8620	−2.1402
	Avg	**−3.8621**	−3.8627	−3.5321	−3.8544	−3.7232	−3.8620	−2.5540
	Std	$\mathbf{4.48 \times 10^{-4}}$	1.7532×10^{-3}	4.4886×10^{-2}	2.5942×10^{-3}	1.5848×10^{-1}	2.2204×10^{-16}	2.0252×10^{-6}
	Rank	**1**	2	3	5	6	5	7
F20	Best	−3.3319	**−3.3220**	−3.0374	−3.1078	−2.5427	−3.1376	−2.1219
	Worst	−3.3220	**−3.3220**	−1.7333	−2.9250	−1.5969	−3.1376	−1.8404
	Avg	−3.3243	**−3.3220**	−2.4687	−3.0980	−2.2673	-3.2483×10	−1.9994
	Std	1.12×10^{-9}	**0**	3.4222×10^{-1}	6.7225×10^{-2}	4.0137×10^{-1}	1.0097×10^{-1}	4.6459×10^{-6}
	Rank	2	**1**	3	4	5	6	7
F21	Best	**−10.2401**	−10.1532	−10.1532	−2.4679	−2.3694	−10.1532	−10.1528
	Worst	**−10.2401**	−10.1532	−10.1532	−2.0438	-7.0292×10^{-1}	−2.6305	−2.6828
	Avg	**−10.2401**	−10.1532	−10.1532	−2.2321	−1.7882	−5.1049	−6.6380
	Std	**0**	0	0	8.5402×10^{-1}	1.9342×10	3.0715	3.3570
	Rank	**1**	2	2	3	5	4	6
	Total Rank	22	30	45	61	86	102	120
	Achieved Rank	1.047	1.428	2.142	2.904	4.095	4.857	5.714

the RBFNN using the AOASC-DTBO algorithm and evaluates the cost function using the normalised mean squared error. At each iteration, the updated weights and biases are evaluated based on the cost function, which is:

$$\text{NRMSE} = \frac{1}{\tilde{A}}\sqrt{\frac{1}{D}\sum_{z=1}^{D}(A_i - P_z)^2} \tag{44}$$

where NRMSE is the normalised root mean square error (RMSE), A_i and P_z are the actual and predicted PV and wind generation. $\tilde{A} = [\max(A) - \min(A)]$ and D is the number of data samples. This entire process is repeated 20 times, and after the 20 runs, the best trained model is selected for wind and PV power forecasting.

5 | Results and Analysis

In this section, the AOASC-DTBO algorithm is evaluated and compared with the traditional DTBO and other state of the art optimisation methods for both single- and multi-objective dispatch problems. All simulations are performed using MATLAB. Section 5.1 presents the wind and PV forecasting results obtained using the AOASC-DTBO-trained evolutionary RBFNN. The forecasted data is subsequently applied to the HDEED problem. Sections 5.2–5.5 assess the effectiveness of the proposed AOASC-DTBO in solving HDEED problems using various IEEE benchmark test networks. To ensure result reliability, each optimisation method was executed 30 times to account for stochastic effects.

5.1 | Wind and PV Forecasting

Accurate energy prediction is essential for efficient market operations and effective generation scheduling [55], particularly in the context of wind and solar energy forecasting [56]. Reliable predictions of photovoltaic (PV) and wind power lead to reduced

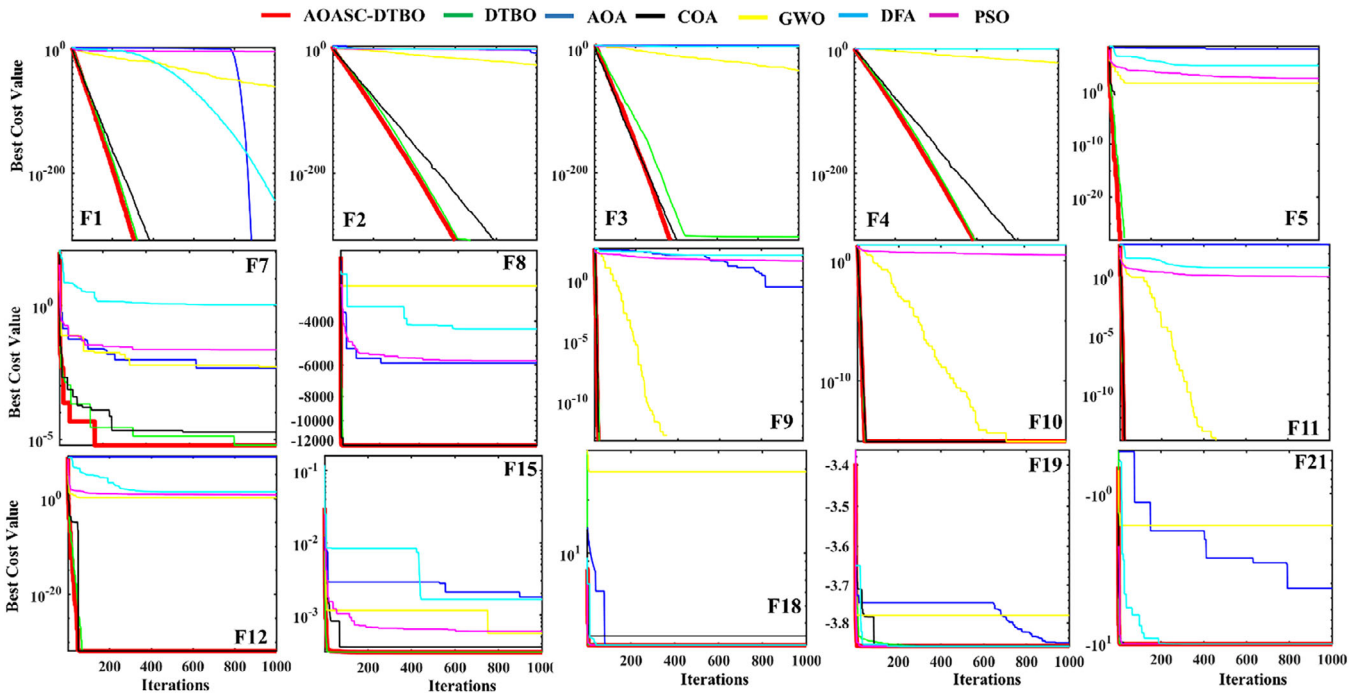

FIGURE 2 | Best cost value versus iterations for standard function.

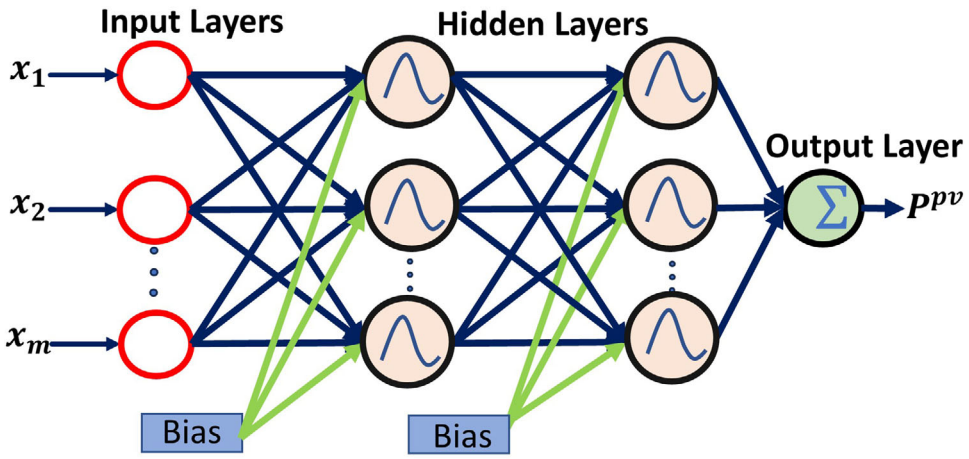

FIGURE 3 | Radial basis function neural network.

reserve requirements, enhanced grid stability and lower dispatch costs. In contrast, poor prediction accuracy results in operational inefficiencies and higher dispatch costs. To improve prediction accuracy, the AOASC-DTBO algorithm is used to train an RBFNN for short-term wind and solar power forecasting. Furthermore, the prediction accuracy for wind and solar PV power is quantitatively evaluated using metrics such as RMSE, relative error (RE) and R^2, as discussed in Section 5.1.3.

5.1.1 | Wind Power Prediction

The dataset used for wind power prediction includes wind speed and wind direction as input features, with wind power generation as the output feature. The dataset is taken from [57], and the proposed AOASC-DTBO trained neural network is used to predict wind power. For further verification results are compared with DTBONN, PSONN, AOANN and BMONN architectures. Figure 5a displays a comparison of actual and predicted wind power using five techniques. The simulation results indicate that the proposed technique has excellent prediction capabilities, surpassing the compared models. Figure 5b represents hourly samples taken from forecasted wind power, which served as input data for the HDEED problem. These hourly samples, derived from the AOASC-DTBO-trained neural network model, closely align with actual wind power data, offering a more accurate and practical approach to optimising power generation while reducing both costs and environmental impact.

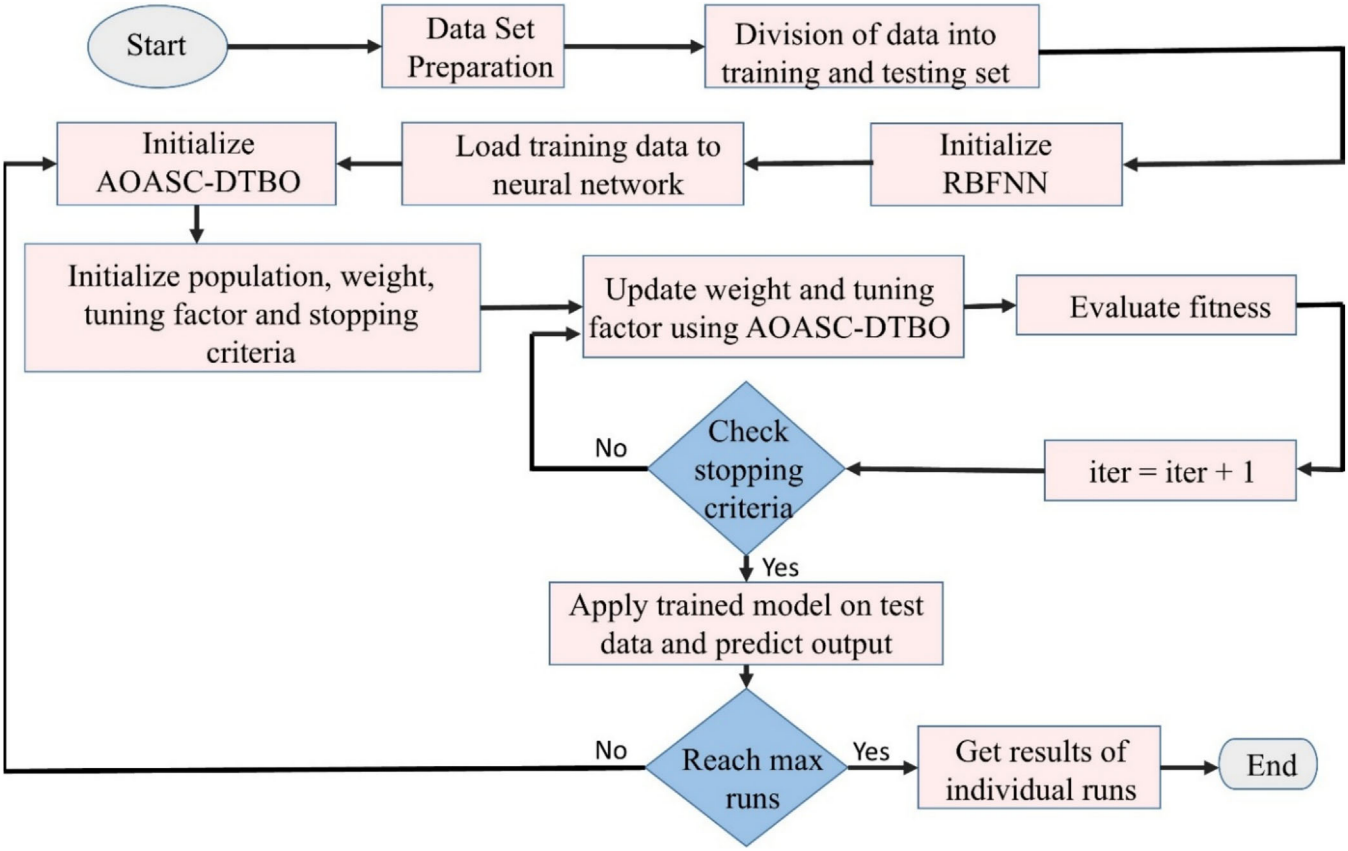

FIGURE 4 | Flowchart of proposed hybrid evolutionary neural network.

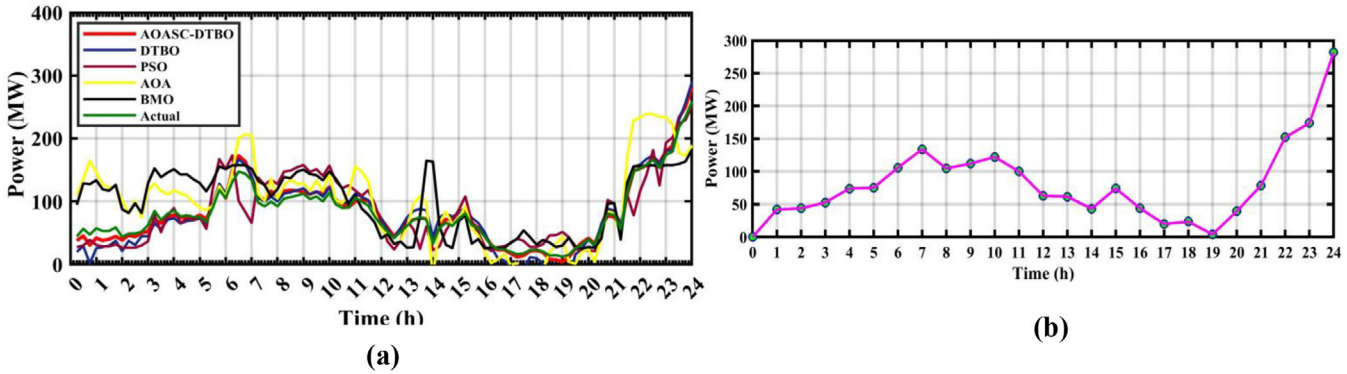

FIGURE 5 | (a) Wind power prediction using hybrid evolutionary neural networks and (b) predicted power for the HDEED problem.

5.1.2 | Solar Power Prediction

The dataset used in this study is taken from [58]. The dataset contains two files. The first dataset has DC and AC power generation data, and the other contains sensor readings for module temperature, irradiance and ambient temperature. These two files were merged using MATLAB code to create a solar power prediction dataset, with measurements taken every 15 min. The proposed evolutionary neural network is employed to predict PV power, and the results are presented in Figure 6a. These results demonstrate that the AOASC-DTBO-trained neural network achieves the highest prediction accuracy, outperforming all other methods. Figure 6b illustrates hourly samples derived from the forecasted solar power, which are subsequently used as input data for the HDEED problem.

5.1.3 | Statistical Indicators for Regression

The performance of different prediction models for wind and solar prediction is evaluated using metrics such as RMSE, relative

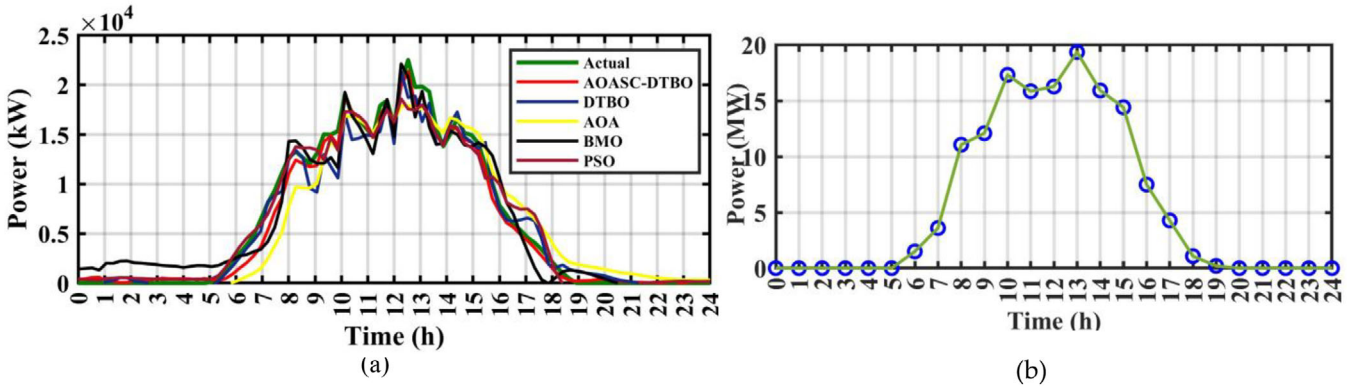

FIGURE 6 | (a) Solar power prediction using various hybrid evolutionary neural networks. (b) Predicted power for the HDEED problem.

TABLE 2 | Statistical indicators for wind and PV forecasting.

		Training indicators			Testing indicators			
	Models	**RE**	**RMSE**	**R^2**	**RE**	**RMSE**	**R^2**	**Fitness function**
Wind power prediction	AOASC-DTBONN	0.00127	9.0313	0.9814	0.0569	28.6747	0.9194	0.1331
	DTBONN	0.0170	25.6071	0.9657	0.1065	61.2748	0.7213	0.2452
	BMONN	0.0959	32.5220	0.8278	0.2318	107.934	0.5712	0.3266
	AOANN	0.0356	16.9534	0.8961	0.1135	59.1465	0.9194	0.1537
	PSONN	0.0049	15.3396	0.8918	0.0642	32.7880	0.8722	0.1889
PV power prediction	AOASC-DTBONN	0.0210	94.9000	0.9795	0.0612	198.931	0.9696	0.0722
	DTBONN	0.0461	166.478	0.8835	0.1285	260.853	0.8140	0.1431
	BMONN	0.0459	148.506	0.7441	0.1148	292.418	0.6777	0.3420
	AOANN	0.0329	133.241	0.9238	0.1111	233.832	0.8751	0.0820
	PSONN	0.0236	102.329	0.9613	0.0740	223.870	0.9116	0.0732

error (RE) and R^2. These statistical measures are commonly used to determine model accuracy. For instance, higher R^2 values and lower RE and RMSE values generally indicate better model performance.

$$RMSE = \sqrt{\frac{\sum_{j=1}^{d} \left(T_j - P_j\right)^2}{n}} \tag{45}$$

$$RE = \sum_{j=1}^{d} \left| \frac{T_j - P_j}{T_j} \right| \tag{46}$$

$$R^2 = 1 - \frac{\sum_{j=1}^{d} \left(T_j - P_j\right)^2}{\sum_{j=1}^{d} \left(T_j - \overline{T_j}\right)^2} \tag{47}$$

where T_j is the true value and p_j is the predicted value. $\overline{T_j}$ is the mean of the true value, and d is the number of data samples.

The study assessed the performance of various prediction models using metrics such as RMSE, RE and R^2. Table 2 presents the results, indicating that the proposed AOASC-DTBONN model demonstrated the highest R^2 values and the lowest RMSE values. This indicates that the AOASC-DTBONN model outperforms the other models. The PSO-trained ANN model also demonstrated good prediction efficiency, but slightly lower than that of AOASC-DTBO.

5.2 | Case I: DEED for 10-Unit System

5.2.1 | Single Objective Dispatch for 10-Unit System

In this experiment, the proposed AOASC-DTBO algorithm was evaluated on a 10-unit system with a load of 2000 MW. The system data was obtained from [59] and the results presented are the best outcomes from 30 trials. Renewable integration was not considered in this case. The dispatch results are presented in Table 3. The tabular results show that the proposed AOASC-DTBO achieved an optimum fuel cost of 111497.6198 $/h outperforming DTBO, which obtained the fuel cost of 111498.0542 $/h. The convergence curve in Figure 7a also shows that the proposed algorithm outperformed other algorithms in achieving the optimum fuel cost value with the lowest violation. Furthermore, the results in Table 4 indicate that the AOASC-DTBO algorithm achieved the best total emission value of 3932.2143 tonne/h with the lowest

TABLE 3 | Dispatch results for the fuel cost of Case I.

Algorithm	AOASC-DTBO	DTBO	PSO	BMO	AOA
P1	55.0000	54.9983	55.0000	55.0000	55.0000
P2	80.0000	80.0000	80.0000	80.0000	80.0000
P3	106.3882	106.9783	107.5730	120.0000	108.0000
P4	101.9411	101.8839	100.3759	101.1538	101.1538
P5	81.3685	81.0934	81.7096	81.0282	81.0282
P6	82.3380	82.2266	82.3899	70.0000	82.0000
P7	300.0000	299.9932	300.0000	300.0000	300.0000
P8	340.0000	339.8623	340.0000	340.0000	340.0000
P9	470.0000	470.0000	470.0000	470.0000	470.0000
P10	470.0000	470.0000	470.0000	470.0000	470.0000
Transmission loss	**87.0325**	**87.0434**	**87.0593**	**87.1497**	**87.0539**
Penalty value	**0**	$\mathbf{1.0 \times 10^{-7}}$	$\mathbf{1.02 \times 10^{-5}}$	$\mathbf{1.02 \times 10^{-5}}$	$\mathbf{1.21 \times 10^{-6}}$
Fuel value	**111497.6198**	**111498.0542**	**111497.9934**	**111539.0986**	**111506.6794**

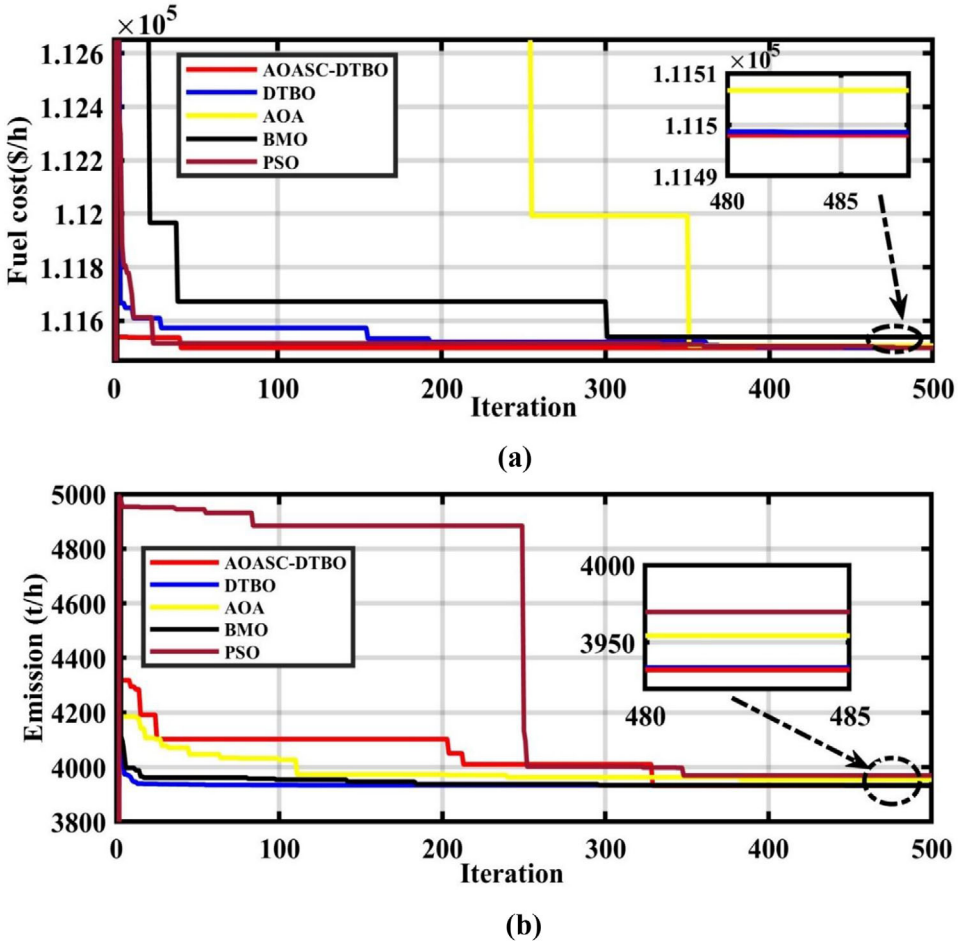

FIGURE 7 | Convergence curves for Case I: (a) fuel cost and (b) emissions.

TABLE 4 | Dispatch results for the emission of Case I.

Algorithm	AOASC-DTBO	DTBO	PSO	BMO	AOA
P1	55.0000	55.0000	55.0000	55.0000	55.0000
P2	79.8931	80.0000	79.9443	80.0000	80.0000
P3	80.8759	78.5312	80.7366	87.3096	73.3181
P4	81.0840	84.1200	80.7974	67.1256	70.6878
P5	160.0000	160.0000	160.0000	160.0000	160.0000
P6	240.0000	240.0000	240.0000	240.0000	240.0000
P7	293.5912	300.0000	293.8110	300.0000	285.5555
P8	298.3664	296.8144	299.4208	310.5100	282.9650
P9	397.4593	398.3287	395.5783	390.7850	415.7374
P10	395.3386	388.7630	396.3216	392.6568	420.5932
Transmission loss	**81.6087**	**81.4901**	**81.6097**	**81.8149**	**82.7149**
Penalty value	**0**	$\mathbf{1.0 \times 10^{-7}}$	$\mathbf{1.0 \times 10^{-5}}$	$\mathbf{1.25 \times 10^{-6}}$	$\mathbf{1.26 \times 10^{-5}}$
Emission value	**3932.2143**	**3933.7674**	**3932.4258**	**3951.5155**	**3954.4536**

TABLE 5 | Statistical results for 10-unit system.

Objective	Algorithm	Best	Worst	Average	Std
Fuel cost $	AOASC-DTBO	111497.619	111497.751	111497.714	0.051
	DTBO	111498.054	111521.142	111510.133	2.106
	PSO	111497.993	111499.213	111498.321	0.0876
	BMO	111539.098	111557.927	111551.236	1.472
	AOA	111506.679	111578.427	111543.159	3.173
Emission tonne/h	AOASC-DTBO	3932.2143	3932.389	3932.3469	0.048
	DTBO	3933.7674	3941.238	3935.194	0.810
	PSO	3932.4258	3936.327	3934.216	0.622
	BMO	3951.5155	3981.124	3966.194	5.127
	AOA	3954.4536	3974.528	3961.140	3.125

violation. The results are further supported by the convergence curve shown in Figure 7b and the statistical analysis presented in Table 5.

5.2.2 | Multi-Objective Dispatch for 10-Unit System

Table 6 displays the optimal solutions for multi-objective dispatch of case I. The table compares the performance of the AOASC-DTBO, DTBO, AOA, OGHS [60], BMO and NGPSO [59] for multi-objective dispatch of a 10-unit system. According to Table 6, the multi-objective AOASC-DTBO algorithm generated solutions that resulted in both lower fuel costs and reduced total emissions compared to other algorithms. The best compromise solutions identified by the AOASC-DTBO algorithm provide the lowest fuel cost of 112800.1033 $/h and a total emission of 4196.399043 tonne/h indicating a superior efficiency in balancing both cost and emission. In comparison, the DTBO algorithm achieved a fuel cost of 113158.3154 $/h and a total emission of 4192.29507 tonne/h while the AOA algorithm yields the highest fuel cost of 114,832.099 $/h and a lower emission cost of 4063.644 tonne/h. The comparison shows that AOASC-DTBO offers a better balance of fuel cost and emission reduction compared to the other algorithm. Figure 8 displays the PFs and BCS generated by the AOASC-DTBO. The solution set of the AOASC-DTBO algorithm had a more uniform distribution compared to the DTBO algorithm, resulting in a smoother distribution of PFs.

5.3 | Case II: DEED for 40 Unit System

5.3.1 | Single Objective Dispatch for 40-Unit System

In this section, a 40-unit system was evaluated using various algorithms, including the proposed AOASC-DTBO. The considered load demand was 10,500 MW. The experiment was conducted considering a population size of 1500 and a maximum iteration limit of 1500, with data obtained from [59]. Table 7 summarises

TABLE 6 | BCS of multi-objective AOASC-DTBO and DTBO for Case I.

Algorithm	AOASC-DTBO	DTBO	AOA	OGHS	BMO	NGPSO
P1	54.7587	55.0000	55.0000	55.00	54.2881	55
P2	79.8162	80.0000	80.0000	79.998	80.0000	80
P3	88.2610	94.4747	79.9543	85.2236	82.2723	81.2398
P4	86.7824	76.7636	60.5116	84.3022	86.2419	80.833429
P5	134.7648	124.7467	160.0000	137.1243	152.3370	160
P6	143.4135	166.0790	190.8067	155.8936	165.5609	235.0087
P7	284.5849	276.3949	300.0000	299.9981	294.2950	289.3507
P8	305.6261	313.1160	340.0000	315.726	312.2843	297.4542
P9	450.9636	430.3213	372.4978	434.9409	428.5518	401.50728
P10	453.5487	470.0000	444.8719	436.0067	427.8895	401.42752
Fuel cost ($/h)	**112800.103**	**113158.315**	**114832.099**	**1.131e5**	**113757.784**	**116179.648**
Emission cost (t/h)	**4194.399**	**4192.295**	**4063.644**	**4144.408**	**4086.3952**	**3939.227**

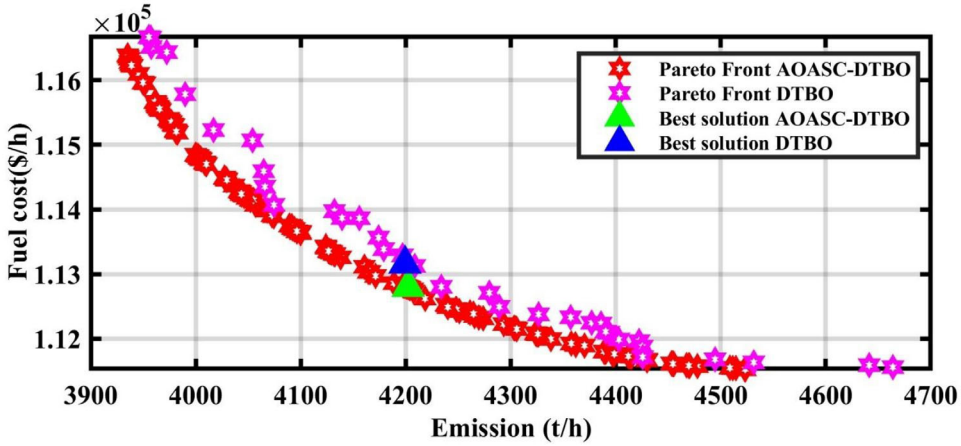

FIGURE 8 | PFs and BCSs of multi-objective AOASC-DTBO and DTBO for 10-unit system.

the optimal fuel cost values achieved by all algorithms, with the proposed AOASC-DTBO achieving the lowest fuel cost of 121,413.6845 $/h. The DTBOB algorithm also performed well, reaching a fuel cost of 122,520.1038 $/h. For total emission minimisation, AOASC-DTBO achieved the best result of 176,681.4367 tonne/h (Table 8). The convergence curves for both cost and emission minimisation are presented in Figures 9 and 10. Statistical analysis further indicates that the AOASC-DTBO algorithm is the most efficient among the studied algorithms (Table 9).

5.3.2 | Multi-Objective Dispatch for 40 Unit System

Table 10 presents the optimal solutions for multi-objective dispatch of case II. The best compromise solutions identified by the AOASC-DTBO algorithm provide the lowest fuel cost of 127201.5202 $/h and a total emission of 188588.7949 tonne/h, indicating a superior efficiency in balancing both cost and emission. In comparison, the DTBO algorithm achieved a fuel cost of 128328.7612 $/h and a total emission of 189796.6436 tonne/h while the AOA algorithm yields the highest fuel cost of 129269.2392 $/h and the lowest emission of 187417.2173 tonne/h. Furthermore, Figure 11 displays the PFs and BCS generated by the AOASC-DTBO and DTBO algorithms. The solution set of the AOASC-DTBO algorithm had a more uniform distribution compared to the DTBO algorithm, resulting in better results.

5.4 | Case III: HDEED for a 10-Unit System

In Case III, the proposed AOASC-DTBO algorithm was utilised to solve HDEED over 24 h. Case III considers two scenarios: Situation 1, which includes 10 thermal units. Situation 2: which consists of 10 thermal units, 1 wind unit and 1 PV unit. The hourly wind and PV forecasted power are shown in Figures 5b and 6b, respectively. Transmission loss coefficients were calculated using load flow analysis using MATPOWER, and the technical data and load demand were obtained from [1].

5.4.1 | Dispatch With and Without Renewable Energy

The results for dynamic dispatch, considering both scenarios (with and without renewable energy), are presented in Figure 12.

TABLE 7 | Dispatch results for the fuel cost of case II.

Algorithm	AOASC-DTBO	DTBO	PSO	AOA	BMO
P1	111.7925	81.0747	114.0000	113.9122	114.0000
P2	111.7610	113.5139	74.5316	112.6995	108.4105
P3	119.8464	97.6803	120.0000	98.5194	120.0000
P4	180.8434	183.7102	190.0000	182.7547	190.0000
P5	96.9132	96.9985	79.0743	92.3976	97.0000
P6	140.0000	139.9545	140.0000	139.9560	140.0000
P7	279.4100	300.0000	300.0000	267.3645	294.0596
P8	291.8877	298.2920	300.0000	290.7340	234.5768
P9	290.5785	289.0410	300.0000	288.5487	300.0000
P10	131.3361	131.0163	130.0000	205.0946	245.6187
P11	94.9832	94.0191	94.0000	97.7234	153.1315
P12	169.8481	94.3288	94.0000	94.1077	196.2309
P13	125.8241	304.7786	125.0000	125.2230	398.0080
P14	305.8713	305.1759	422.2368	304.7200	324.9377
P15	304.8888	395.3959	500.0000	394.2797	431.5540
P16	394.3828	304.6502	133.8991	394.2838	260.8538
P17	489.4839	492.4768	500.0000	490.2210	497.3586
P18	490.1315	490.3354	410.3790	489.4500	500.0000
P19	511.3783	511.7794	538.7182	512.8458	550.0000
P20	514.8562	513.5973	550.0000	512.3042	550.0000
P21	541.5688	536.4361	550.0000	527.4048	513.5819
P22	531.5488	549.9416	550.0000	526.4016	283.5900
P23	524.4317	523.5534	538.5468	524.3280	438.8656
P24	530.7627	526.2961	538.5468	527.4760	550.0000
P25	524.3284	525.2444	550.0000	526.0408	453.8114
P26	529.4505	549.5761	550.0000	525.5536	516.5667
P27	11.0716	11.2661	10.0000	13.1846	32.1307
P28	12.5248	11.9239	29.8964	12.3550	64.4960
P29	11.6720	10.6852	10.0000	15.2493	61.4618
P30	94.2655	88.7904	97.0000	95.5222	97.0000
P31	189.9092	190.0000	190.0000	190.0000	190.0000
P32	190.0000	189.9655	190.0000	189.9827	185.8086
P33	189.9299	189.9723	158.8898	190.0000	190.0000
P34	199.9765	197.0312	163.9020	199.8725	200.0000
P35	199.7679	179.5630	200.0000	187.6397	141.9095
P36	183.2943	189.1959	200.0000	200.0000	181.8509
P37	109.5713	93.2567	110.0000	109.9340	110.0000
P38	110.0000	97.5326	110.0000	109.9233	48.3835
P39	109.9954	89.3998	110.0000	110.0000	47.0658
P40	550.0000	512.5532	550.0000	512.0578	550.0000
Penalty value	**0**	$\mathbf{1.0 \times 10^{-9}}$	$\mathbf{1.04 \times 10^{-5}}$	$\mathbf{1.38 \times 10^{-6}}$	$\mathbf{1.6 \times 10^{-7}}$
Cost value	**121413.6845**	**122520.1038**	**125433.7046**	**121915.758**	**132642.2845**

TABLE 8 | Dispatch results for the emission of Case II.

Algorithm	AOASC-DTBO	DTBO	PSO	BMO	AOA
P1	113.8683	113.8877	114.0000	114.0000	113.8862
P2	113.9802	114.0000	114.0000	114.0000	113.9804
P3	119.9541	119.8810	120.0000	60.0000	119.4512
P4	168.3232	167.6665	190.0000	190.0000	170.0610
P5	96.9678	96.9359	97.0000	47.0000	96.9904
P6	126.3087	124.4018	140.0000	140.0000	124.6750
P7	299.5508	297.4341	300.0000	300.0000	299.9939
P8	298.5879	296.1611	300.0000	300.0000	298.2286
P9	295.5735	296.9869	300.0000	300.0000	294.2224
P10	132.1144	138.4593	130.0000	130.7782	140.2524
P11	298.6786	299.8476	292.8599	296.9873	298.0758
P12	298.2426	296.7315	295.0737	296.9698	296.2621
P13	434.3461	433.0198	425.1045	433.2373	431.7178
P14	422.9193	423.9345	415.5268	416.5770	419.5765
P15	419.8715	418.2565	410.9591	417.2413	422.9518
P16	421.7811	420.5382	410.7560	418.1172	423.3651
P17	439.4378	440.7860	439.4820	500.0000	437.6726
P18	439.1813	442.0273	434.2008	433.4387	440.1097
P19	438.6446	443.4343	430.9295	439.8991	439.2075
P20	437.2548	440.2835	433.7884	434.2201	439.1182
P21	438.9818	437.2392	429.8951	432.9534	441.7651
P22	438.4240	440.3073	431.1162	441.4978	438.7813
P23	439.0487	444.2320	430.3811	439.5742	440.1021
P24	437.0578	442.1642	434.2581	439.3102	439.7169
P25	441.1924	443.1275	424.7006	439.1494	439.3224
P26	442.8270	440.1967	428.1792	439.7743	441.4701
P27	26.2212	29.8486	10.0000	10.0000	33.4251
P28	31.0139	23.9769	10.0000	31.9281	28.5776
P29	34.5588	20.1615	150.0000	28.1064	29.4530
P30	97.0000	97.0000	47.0000	97.0000	96.9926
P31	171.9699	174.1739	190.0000	169.2801	171.7342
P32	172.6663	171.4363	168.1770	190.0000	171.1469
P33	170.6963	174.1239	190.0000	190.0000	172.0850
P34	200.0000	200.0000	200.0000	200.0000	200.0000
P35	200.0000	200.0000	200.0000	200.0000	200.0000
P36	200.0000	200.0000	200.0000	200.0000	200.0000
P37	99.2388	98.8681	110.0000	110.0000	97.6656
P38	103.6371	97.5765	110.0000	110.0000	102.2294
P39	100.4876	101.8587	110.0000	110.0000	97.9201
P40	439.4077	439.1097	432.6924	439.1483	437.8178
Penalty value	**0**	**1.31×10^{-7}**	**1.0×10^{-6}**	**1.1×10^{-8}**	**1.7×10^{-8}**
Emission value	**176681.4367**	**177111.8441**	**216369.7021**	**197703.4185**	**176899.8361**

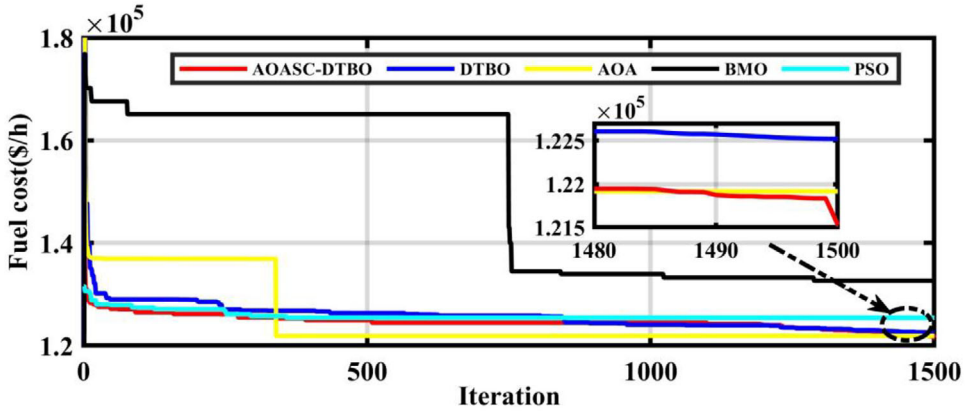

FIGURE 9 | Convergence curve for fuel cost of case II.

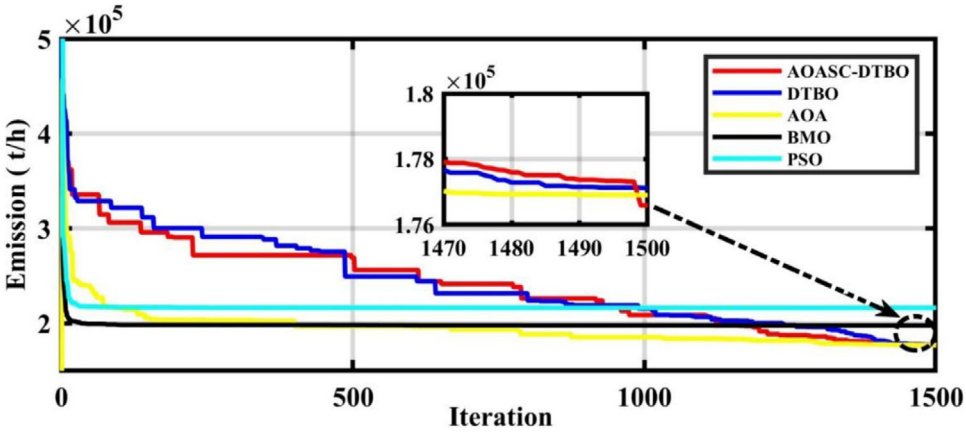

FIGURE 10 | Convergence curve for emission of Case II.

TABLE 9 | Statistical results for 40-unit system.

Objective	Algorithm	Best	Worst	Average	Std
Fuel cost	**AOASC-DTBO**	121413.6845	121711.528	121697.481	120.168
	DTBO	122520.1038	122921.539	122729.291	320.147
	PSO	125433.7046	125541.295	125502.174	201.692
	BMO	121915.758	122601.125	122570.918	600.185
	AOA	132642.2845	133208.352	132965.283	814.139
Emission	**AOASC-DTBO**	176681.436	176999.359	176691.249	31.017
	DTBO	177111.844	177251.293	177204.831	102.134
	PSO	216369.702	216396.169	216390.361	29.169
	BMO	197703.418	198192.492	197921.120	170.264
	AOA	176899.836	178652.194	177526.273	505.863

The PFs and BCS obtained by the AOASC-DTBO algorithm for the first scenario (without renewable energy units) are presented in Figure 12a, while the results for the second scenario (with renewable energy) are displayed in Figure 12b. The figure displays hourly Pareto frontiers for an entire day, meaning there are 24 Pareto fronts, each representing a different instance of the HDDED throughout the day. Table 11 presents the optimal hourly dispatch results from the AOASC-DTBO algorithm. Figure 13a displays a stacked histogram of the total power generation across the 10 units, where each bar represents the power output of a single unit. This histogram indicates that the power output from the dispatch units consistently meets the combined

TABLE 10 | BCS for the 40-unit system.

Algorithm	AOASC-DTBO	DTBO	AOA	BMO	PSO
P1	111.2336	111.0044	110.1253	113.8815	110.5705
P2	111.9410	113.4750	114.0000	110.1511	109.3459
P3	119.2446	120.0000	119.5049	118.7390	117.9321
P4	182.4524	149.8414	179.0548	181.6666	188.4046
P5	94.7145	96.3030	92.1243	96.2330	95.8629
P6	113.2064	105.6933	136.1836	137.7312	125.5941
P7	292.9554	294.3336	299.2321	299.8434	298.0977
P8	285.7419	296.2685	281.6523	288.1388	300.0000
P9	285.3226	287.1062	295.4761	289.1384	284.1044
P10	132.9001	132.2548	134.2740	131.2078	130.9151
P11	314.1158	323.0074	295.3838	318.5115	319.5561
P12	247.1847	322.9441	291.5641	316.8974	242.6577
P13	309.6383	388.0005	305.6156	397.6496	394.8748
P14	394.2914	391.4188	316.5475	400.6387	396.9845
P15	397.8692	428.6568	392.2257	395.5951	394.0968
P16	393.3733	418.2863	305.5025	397.5465	394.4653
P17	486.8697	473.3743	485.8563	482.9505	489.0877
P18	488.7766	450.7581	493.1221	482.9040	492.8760
P19	503.5343	457.7435	416.8113	426.4043	424.8909
P20	447.5800	460.7455	506.2974	438.3144	421.5566
P21	450.6810	433.8216	517.1056	436.7599	434.0693
P22	523.6321	437.1200	520.1650	445.1665	443.2731
P23	518.8770	466.0140	433.5846	448.9572	457.6837
P24	440.4355	443.3879	520.7402	436.9205	438.5355
P25	433.6907	433.5801	446.4677	455.4506	521.6642
P26	437.6032	436.1766	509.4292	434.7125	509.4313
P27	12.1101	14.9562	13.4674	12.5528	10.0000
P28	11.5235	17.3680	10.8935	10.4947	10.0295
P29	13.9585	13.0003	10.0000	11.6795	11.8330
P30	94.7795	89.7326	96.2167	94.5506	96.8321
P31	189.1361	182.7448	190.0000	175.9479	160.1225
P32	167.6282	166.2299	180.4140	176.4601	162.1694
P33	175.1602	186.2040	162.9927	187.4563	186.7756
P34	194.1206	198.8023	199.0898	198.5204	199.8538
P35	200.0000	200.0000	194.8471	198.3356	198.7366
P36	200.0000	198.7621	199.0260	195.6257	198.8867
P37	98.8252	102.2505	109.1863	99.8159	104.8357
P38	106.7237	91.4712	106.7827	99.7949	101.5385
P39	98.1495	109.4759	91.3690	106.5314	101.1638
P40	420.0119	457.9093	417.7144	450.1339	420.9131
Fuel Cost ($/h)	127201.5202	128328.7612	129269.2392	126841.5281	125643.2518
Emission (t/h)	188588.7949	189796.6436	187417.2173	198012.3461	217887.5025

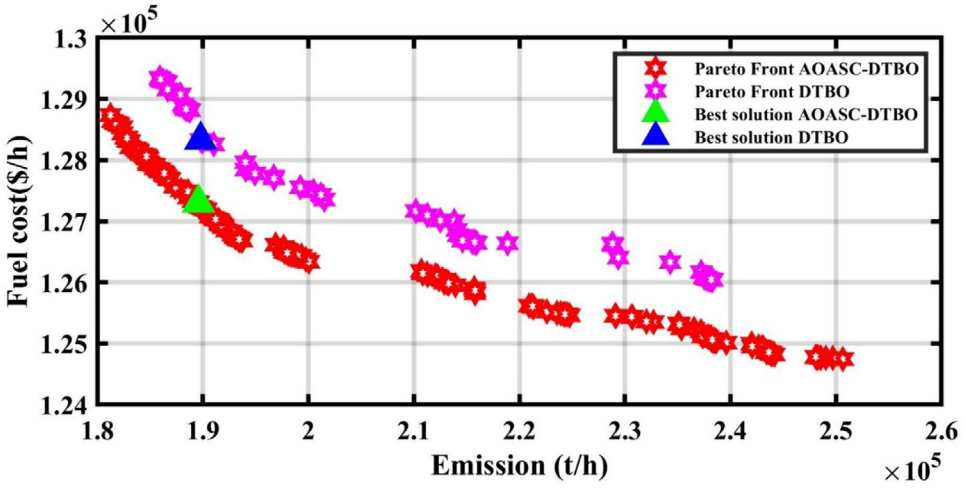

FIGURE 11 | PFs of AOASC-DTBO and DTBO for 40 unit system.

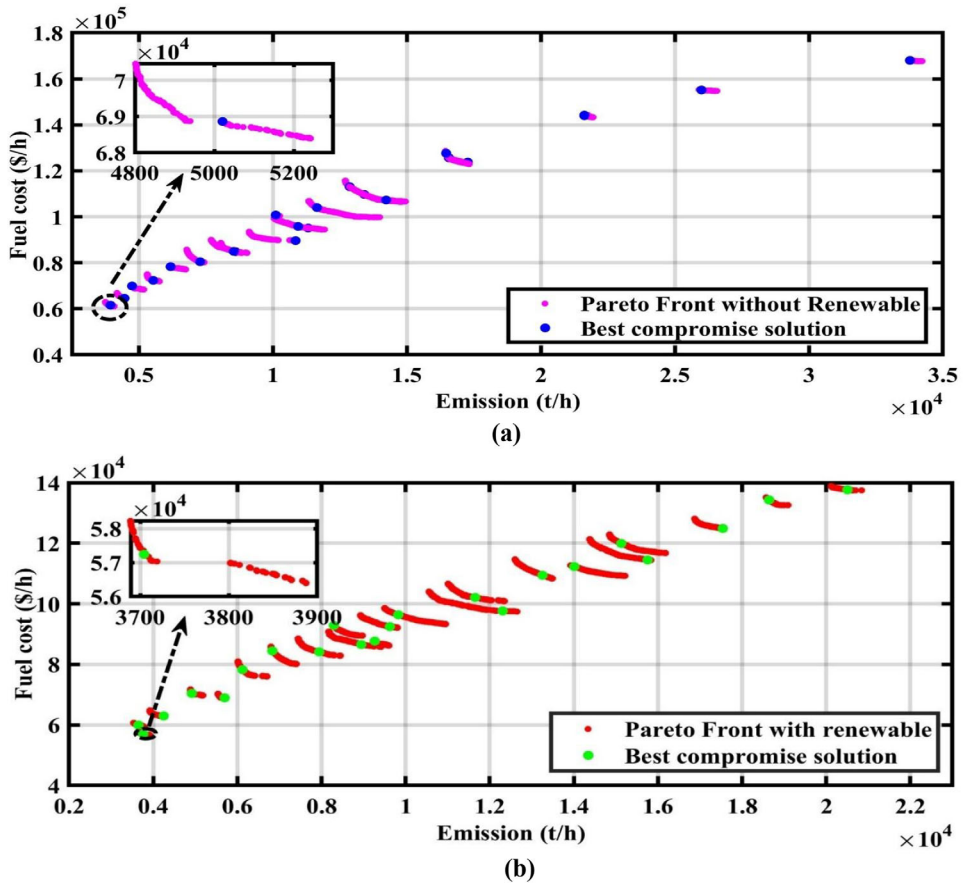

FIGURE 12 | PFs and BCSs for 24 h. (a) Without renewable energy and (b) with renewable energy.

transmission loss and load demand. Additionally, Figure 13b shows the sum of dynamic power generation from the 10 thermal units, 1 wind unit and 1 PV unit, represented in histogram form.

The optimal dispatch results for thermal, wind and PV power output, along with transmission loss, obtained using the AOASC-DTBO algorithm, are presented in Table 12. Table 13 lists the hourly direct costs, as well as the overestimation and underestimation penalty costs for wind and PV, calculated using the AOASC-DTBO algorithm. These penalties and reserve costs account for any discrepancies between the scheduled and available powers from wind and solar energy sources. The direct cost coefficient, underestimation penalty coefficient and overestimation penalty coefficient for both solar and wind were set to 1.1, 1000 and 1000 ($/MWh), respectively.

TABLE 11 | Dispatch results for Case III without renewable.

Time	P1	P2	P3	P4	P5	P6	P7	P8	P9	P10	Loss	Fuel cost	Emission
1	150	135	78.45128	95.72001	123.6915	123.0448	95.91349	119.8818	80	54.06037	19.7353	62392.47	3779.16
2	150	135	98.86462	100.855	147.4887	137.2761	113.2208	114.7695	80	55	22.4196	66181.35	4189.522
3	150	148.517	132.0268	123.3076	188.4466	160	129.8297	119.626	80	55	28.8747	73391.87	5343.369
4	172.294	194.232	162.3038	152.8674	216.5821	159.3841	130	120	80	54.60442	36.1182	84167	6850.618
5	150	157.471	221.1739	202.8674	243	160	130	120	80	55	40.6632	85551.54	8354.685
6	227.4618	234.857	210.4861	216.9061	243	160	130	120	80	55	48.9972	99450.82	9985.13
7	228.5514	228.304	258.7609	252.4178	243	160	130	120	80	55	54.4013	103566.3	11671.98
8	219.9852	222.88	304.7403	299.5925	243	159.9921	129.8653	120	80	54.89889	58.4796	107487.5	14029.88
9	298.2191	302.731	306.1976	300	243	159.9548	129.9453	120	79.96782	54.97605	70.8468	124925.4	15685.19
10	364.0012	364.475	340	300	243	160	130	120	80	55	84.4192	143364.5	21617.18
11	382.845	427.313	340	300	243	160	130	120	80	55	92.0442	154850.5	25402.13
12	433.7286	458.46	340	300	243	160	130	120	80	54.93683	100.1175	167409.8	34123.26
13	353.7286	378.46	337.36	300	242.8675	160	130	120	79.98273	54.10972	84.4841	142966.3	20733.17
14	284.9464	298.46	323.6226	300	243	160	130	120	80	55	71.3578	123632.6	15916.39
15	267.3788	280.021	247.5269	253.2743	242.7318	160	130	120	79.91779	55	59.9307	112679.6	12804.33
16	202.7416	221.7	184.8191	203.2743	241.4569	160	130	120	80	55	44.8581	93743.35	8827.097
17	152.6381	143.903	199.7486	237.5572	240.9024	160	130	120	79.75947	55	40.1299	84721.47	8525.553
18	232.6381	223.903	219.4246	213.9801	243	160	129.6467	120	80	54.96901	49.1518	99196.37	10018.48
19	231.5149	252.586	299.4246	263.9801	243	160	130	120	79.61693	55	59.3784	109445.1	11437.56
20	311.5149	332.586	340	300	243	160	130	120	80	55	76.9993	132018.8	13939.16
21	268.6608	303.385	335.1419	300	243	159.8919	129.9202	120	80	55	71.1836	123671.7	12156.65
22	188.6608	223.385	255.5187	250	224.0624	160	129.9619	119.9735	79.93558	45.33529	48.8626	97105.59	10761.45
23	150	143.385	185.2481	200	174.0624	138.5065	129.4744	120	79.97141	43.30267	32.0116	76864.38	6655.881
24	150	135	115.3472	150	170.7299	141.0255	129.3425	119.9761	53.55766	44.32938	25.3407	68731.99	5020.691
												2537516.2364	**297828.516**

TABLE 12 | Dispatch results for Case III considering renewable integration.

Hour	P1	P2	P3	P4	P5	P6	P7	P8	P9	P10	P wind	P pv	P loss
1	150	135	77.39394	101.8439	122.8551	122.6364	94.30123	84.94194	79.9931	43.5426	42.49143	0	18.9894
2	150	135	76.88753	118.2734	122.5175	122.0721	123.6253	114.8951	80	44.4663	43.97347	0	21.7021
3	150	145.0917	113.6742	114.8494	166.278	160	127.8968	120	80	55	52.80711	0	27.6224
4	150.608	137.0914	159.7288	158.1399	216.278	159.9235	129.2644	120	80	55	73.8	0	33.8938
5	150.3848	135	187.4536	182.7271	243	159.4098	129.9342	120	80	54.1657	75.48109	0	37.6862
6	162.7033	214.179	194.2352	208.2604	242.5065	160	129.0226	120	80	54.8955	106	1.749935	44.7313
7	226.3767	227.0234	185.4798	187.797	243	160	130	120	80	54.9166	133.8	3.49308	48.4275
8	251.0646	258.0762	200.8781	217.7175	243	160	130	119.8499	79.9092	54.9379	105	11.36059	54.7486
9	274.4019	284.4658	269.4266	249.9696	243	159.9427	129.8388	120	79.9088	54.8331	112.1709	12.0471	66.4738
10	304.6332	313.59	306.1642	296.7864	243	159.8645	130	119.9179	80	55	122.9066	17.3	77.3595
11	337.6123	355.5849	333.7063	300	243	160	130	120	80	54.9758	100.4128	15.96921	85.0431
12	393.6112	413.3499	339.9725	300	243	160	130	119.9919	79.9942	55	63	17	94.9144
13	327.7556	333.4177	321.6425	300	243	160	129.9808	120	79.9907	54.9911	61.99978	19.36	80.0890
14	247.7556	278.3124	318.9079	299.9296	242.7052	160	130	120	80	54.4079	43.92874	15.90175	68.5421
15	227.4841	233.8783	244.2148	250.1628	243	160	129.7707	120	80	54.6129	74.42449	14.38874	55.1219
16	152.3735	217.8728	189.2881	200.1628	240.5878	159.9453	129.9488	120	79.6967	55	43.89149	7.997684	42.1468
17	180.9167	206.6479	163.8319	176.2819	222.2476	160	129.6537	120	80	54.9774	20.59367	4.518886	38.9820
18	180.285	220.3315	237.7372	224.4151	243	160	130	120	79.8644	55	25	0.516447	48.3467
19	236.4165	230.137	301.0493	274.4151	243	160	129.9136	120	80	55	5	0.065663	59.7234
20	316.4165	310.137	340	300	243	160	130	120	80	55	40	0	76.9878
21	236.4165	271.2848	315.7594	300	243	160	130	120	80	54.8492	79.97655	0	66.9652
22	156.4165	191.2848	235.7594	250	209.2637	128.7403	130	120	53.6791	44.1688	153	0	44.0621
23	150	135	155.7594	200	164.8751	122.2358	100	119.876	23.7107	14.2471	174.1806	0	28.3419
24	150	135	75.75937	150	114.8751	72.23584	70	89.87595	24.2344	40.3089	282.2302	0	19.7343

TABLE 13 | Dynamic direct, overestimation and underestimation penalties for Case III.

Hour	Direct cost wind ($/h)	Underestimation penalty wind ($/h)	Overestimation penalty wind ($/h)	Direct cost solar ($/h)	Underestimation penalty solar ($/h)	Overestimation penalty solar ($/h)	Thermal cost ($/h)	Total Fuel cost ($/h)	Emission (tonne/h)
1	46.6224	0	38.4022	0	0	0	60365.32	60450.34	3559.881
2	48.3970	0	9.7285	0	0	0	63986.74	64044.86	3959.662
3	58.2959	0	29.6299	0	0	0	71530.33	71618.26	4880.228
4	81.1590	6.9077	0	0	0	0	77454.44	77542.51	6184.871
5	3.6000	0	80.0000	0	0	0	81574.45	81738.05	7062.454
6	116.5981	0	29.8237	1.7529	0	25.2857	86953.53	87126.99	9764.804
7	147.1751	10.4415	0	3.5932	0.6760	0	90876.01	91037.9	10219.75
8	115.5000	0	40.0000	11.4796	0	40.9585	100386.6	100594.5	11004.8
9	123.7421	0	39.2789	12.0500	5.0000	0	117341.6	117521.7	13330.77
10	135.2133	0	82.1199	17.2534	6.6581	0	127759.4	128000.7	16885.95
11	110.4491	0	30.8231	15.9991	0	14.9082	137909.1	138081.3	20360.26
12	69.2955	0	9.5922	16.9995	0	72.9497	154625	154793.8	25773.87
13	68.2000	0	47.0000	19.2739	8.6063	0	133683.6	133826.7	18731.56
14	47.9927	0	41.9772	15.6970	22.3041	0	120484.5	120612.5	15061.5
15	81.9491	0	49.9158	14.4920	0	7.1979	100075	100228.5	12517.3
16	48.4000	0	1.0000	7.8267	0	32.6704	86513.15	86603.05	9026.333
17	22.9738	0	88.5286	4.7202	0	44.0167	84631.72	84791.96	7778.555
18	27.3277	0	119.3408	0.5596	52.0380	0	97040.57	97239.83	9688.942
19	5.4860	0	79.7296	0.1973	0.5653	0	113154.6	113240.6	12697.37
20	44.0000	0	39.0000	0	0	0	130294.1	130377.1	18477.13
21	87.9347	0	130.0612	0	0	0	115447.4	115665.4	15229.02
22	167.5562	0	2.3778	0	0	0	86750.49	86920.42	9341.518
23	192.2532	0	77.5632	0	0	0	69555.15	69824.97	5436.952
24	310.4582	0	13.4735	0	0	0	56672.45	56996.38	3802.255
							2365065.3156	**2368878.3392**	**270775.742**

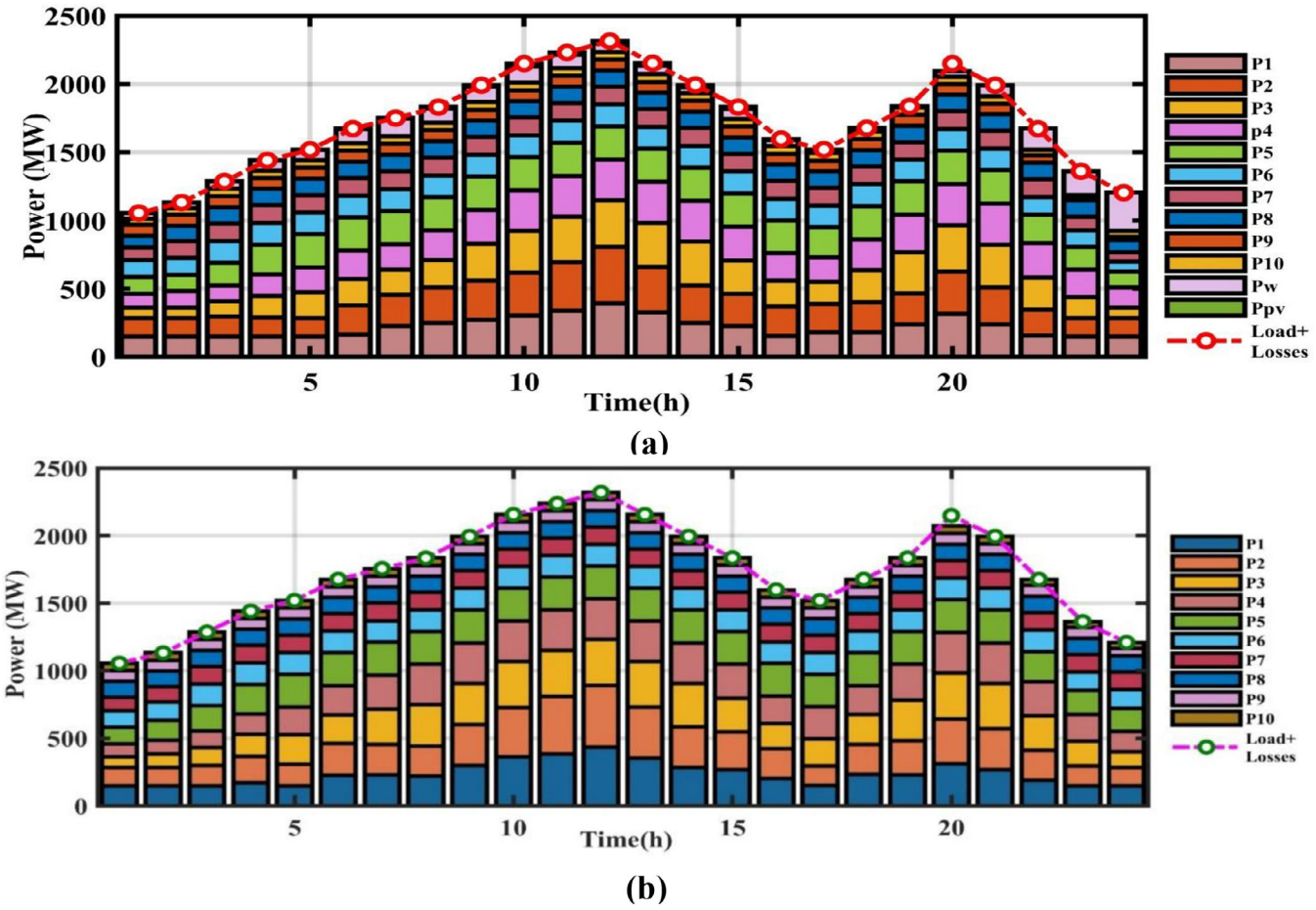

FIGURE 13 | Stacked histogram of dynamic power generation of Case III. (a) Without renewable energy and (b) with renewable energy.

TABLE 14 | Comparative results for Case III.

	Situation 1 (without renewables)						
Cost and emission	**PSO**	**MFO**	**PPSO [61]**	**MONNDE [62]**	**AOA**	**DTBO**	**AOASC-DTBO**
Cost (10^6) ($)	2.59×10^6	2.54×10^6	2.53×10^6	2.56×10^6	2.88×10^6	2.58×10^6	2.53×10^6
Emission (10^5) (tonne)	3.17×10^5	3.07×10^5	3.03×10^5	2.97×10^5	3.60×10^5	3.15×10^5	2.97×10^5
	Situation 2 (with renewables)						
	PSO		**BMO**	**AOA**	**DTBO**		**AOASC-DTBO**
Cost (10^6) ($)	2.47×10^6		2.43×10^6	2.57×10^6	2.51×10^6		2.36×10^6
Emission (10^5) (tonne)	3.10×10^5		2.72×10^5	3.49×10^5	2.93×10^5		2.70×10^5

5.4.2 | Comparative Analysis and Discussion for Case III

Table 14 presents the best compromise solutions obtained by different algorithms for Case III. In Situation 1 (without renewables), the AOASC-DTBO algorithm achieved the minimum cost of 2.53e6, which is 12.1% and 2.31% lower than that of the AOA and PSO algorithms, respectively. Additionally, the AOASC-DTBO algorithm obtained the smallest emission of 2.97e5, which is 17.51% and 5.71% lower than that of the AOA and DTBO algorithms, respectively.

In Situation 2 (considering renewables), the AOASC-DTBO algorithm achieved the minimum cost and emission of 2.36e6 and 2.70e5, respectively. The fuel cost of the AOASC-DTBO algorithm was 6% lower than the DTBO algorithm. Figure 14 shows that using wind and PV power in situation 2 resulted in net savings in cost and reduced emissions. Specifically, the operating cost for situation 1 is \$2537516.2364, and \$2368878.3392 for situation 2, which means net savings of \$168,637.9 per day. Additionally, the emissions for both scenarios were 297828.516 and 270775.742, respectively, resulting in a net reduction of 27052.774 tonnes per day.

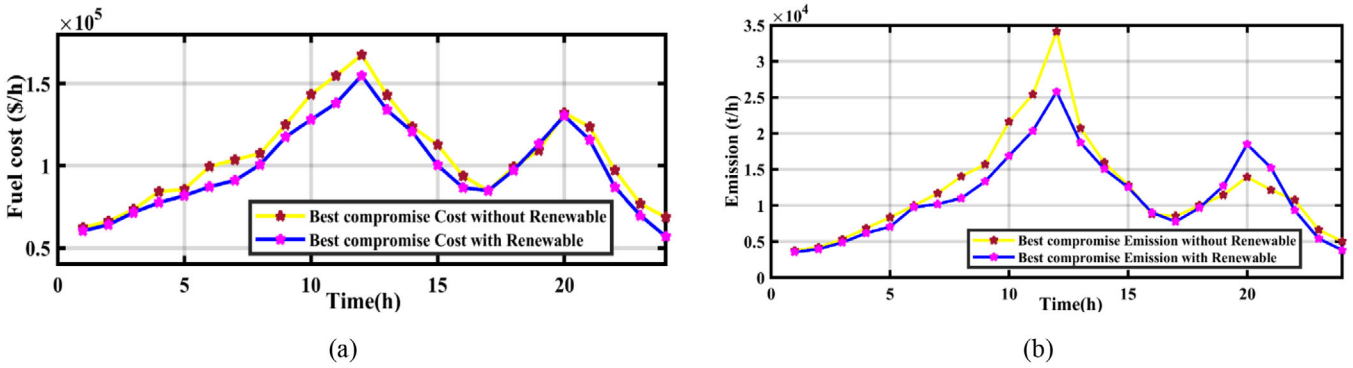

FIGURE 14 | Best compromised cost and emission with and without renewable for Case III. (a) cost and (b) emissions.

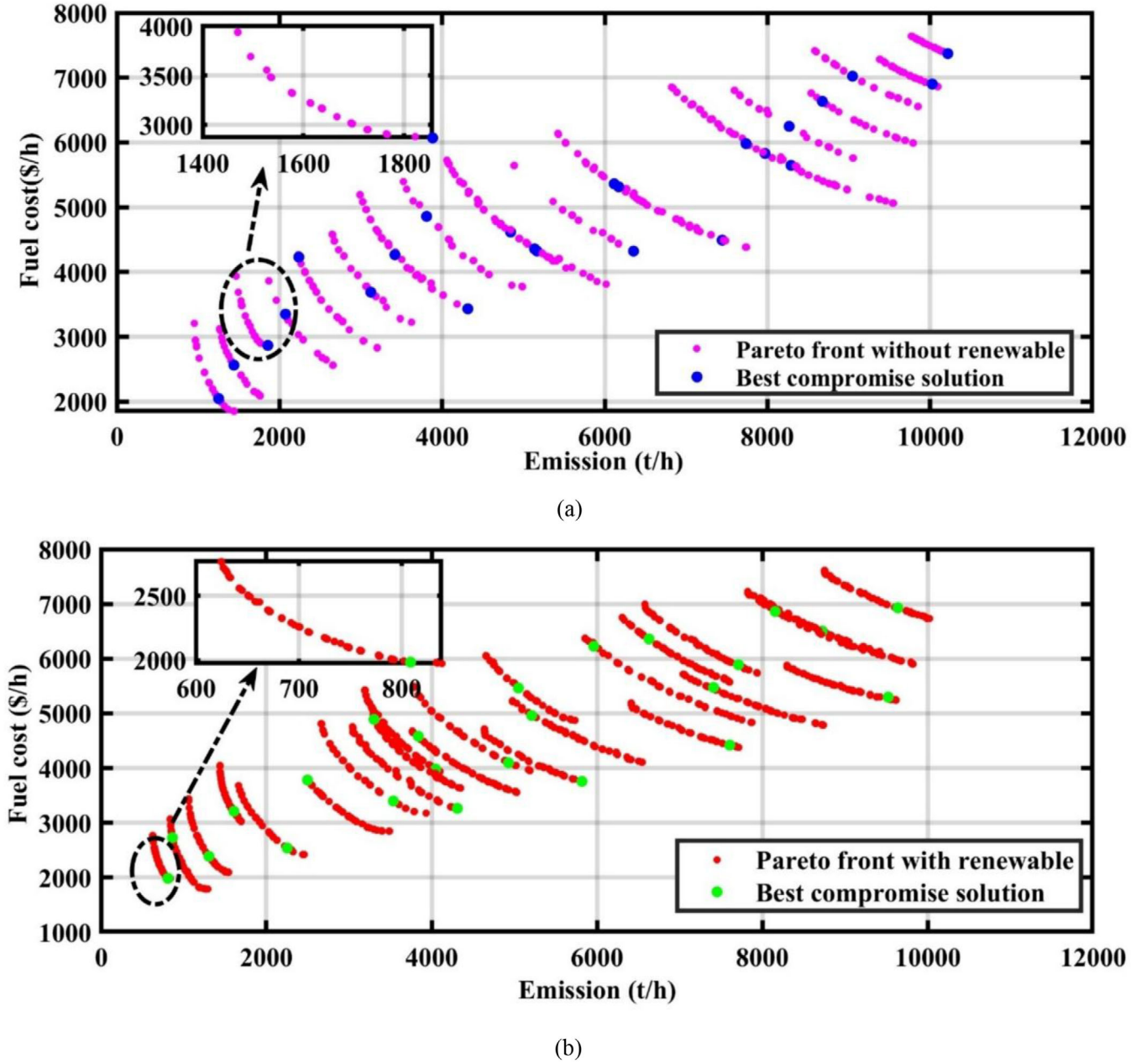

FIGURE 15 | PFs for IEEE 57 bus system. (a) Without renewable energy and (b) with renewable energy.

TABLE 15 | Dispatch results for the IEEE 57 system considering renewables.

Hour	P1	P2	P3	P4	P5	P6	P7	P wind	P pv	P loss
1	151.036	10	62.81138	56.68605	160.4406	47.50815	129.1667	42.13478	0	23.5517
2	213.1129	10	47.81344	27.00205	203.752	22.50815	168.5983	43.92884	0	25.8107
3	269.7228	10	35.4795	12.30091	288.7799	11.35516	208.361	52.7	0	31.4717
4	268.4381	10	84.79489	61.02891	283.1118	36.35516	224.4763	73.8	0	35.5281
5	350.5678	10	57.74665	18.67098	340.8482	15.71191	254.0759	75.1	0	39.6343
6	318.1661	10	107.6457	57.57436	367.3583	40.64161	265.3948	106	1.50923	47.7763
7	375.1245	10	63.87563	14.01646	413.1099	23.92185	317.5514	133.8	3.59349	53.0052
8	377.113	10	89.5967	49.30456	425.6228	48.92185	315.6815	104.6038	11.0964	58.0275
9	377.6018	10	124.1059	94.95983	445.856	72.90536	337.2222	112.01	12.05	66.5068
10	413.5045	10.04716	96.39177	46.57218	547.9126	53.87057	381.5383	122.0646	17.2952	69.9237
11	480.0706	10	101.6009	48.55159	542.0445	76.68076	410	100.05	15.8594	75.1460
12	539.2456	10	129.4603	56.97182	550	65.65167	409.5806	62.90611	16.5111	86.5385
13	448.8521	10	121.5364	75.28642	518.2294	90.3847	400.6424	61.54776	19.36	73.0197
14	408.9241	10	134.9065	92.07351	466.8659	66.80352	349.9184	43.20931	15.855	63.8277
15	354.605	10	120.6824	67.85886	405.8856	64.93457	318.8888	74	14.4467	56.5232
16	350.4986	10.02864	74.01511	22.43778	370.1511	40.05569	279.8534	44	7.54893	43.4027
17	366.3068	10	24.29076	10.19649	416.703	15.05569	252.598	20.01227	4.25906	39.9175
18	416.8575	10	20	10.25671	474.2035	11.15604	306.7309	23.66827	0.99590	44.3610
19	449.4105	10	27.47146	13.44116	538.2545	10.79459	373.5583	4.181118	0.19892	51.8654
20	561.4122	10	41.56248	14.46924	550	20.794	410	39.90582	0	67.1045
21	446.2278	10	91.56248	30.32661	502.6795	45.06937	384.3969	78.43696	0	66.1027
22	326.2278	10.04849	100.6424	80.30096	261.4506	70.03257	279.814	152.2969	0	48.0531
23	208.3188	10	58.34219	42.30519	243.2359	52.1041	176.5033	173.9856	0	35.0666
24	182.5271	10	20.05653	10.05435	173.0921	27.12262	109.9888	282	0	30.8024

5.5 | Case IV: HDEED for IEEE 57-Bus System

In Case IV, the AOASC-DTBO algorithm was applied to address the HDEED problem for the 7-unit IEEE 57-bus test system. The proposed algorithm was utilised to solve HDEED over a 24 h period. Two different scenarios were examined in Case IV. Situation 1 involved 7 thermal units, while Situation 2 included 7 thermal units, 1 wind unit and 1 PV unit. The hourly forecasted wind and PV power values were obtained from Section 5.1 (Figures 5b and 6b). MATPOWER was used to determine the transmission loss coefficients, and the technical data and load demand were obtained from [63].

5.5.1 | Dispatch With and Without Renewable Energy

The results for dynamic dispatch, considering both scenarios with and without renewable energy, are presented in Figure 15. The figure displays hourly Pareto frontiers for an entire day, meaning there are 24 Pareto fronts, each representing a different instance of the HDDED throughout the day. The results for the first scenario (without renewable energy units) are presented in Figure 15a, while the results for the second scenario (with renewable energy) are shown in Figure 15b. Table 15 displays the optimal hourly dispatch results from the AOASC-DTBO algorithm, including the hourly power outputs from thermal, wind and PV units, as well as the transmission loss. Additionally, Table 16 lists the hourly direct costs, overestimation and underestimation penalty costs for both wind and PV, which were calculated using the proposed AOASC-DTBO. These penalties and reserve costs account for discrepancies between the scheduled and available power from wind and solar-based energy sources.

Figure 16a presents a stacked histogram of the total power generation from 7 units, demonstrating that the power generated by the dispatch units consistently meets the combined transmission loss and load demand. Additionally, Figure 16b illustrates the sum of the dynamic power generation from 7 thermal units, 1 wind unit and 1 PV unit in histogram form. The results confirm that the power generated by the dispatch units reliably satisfies both transmission losses and load demand.

5.5.2 | Comparative Analysis and Discussion for Case IV

Table 17 compares the best compromised solutions obtained by different algorithms for Case IV in two distinct scenarios. In Situation 1, the AOASC-DTBO algorithm achieved a fuel

TABLE 16 | Dynamic direct, overestimation and underestimation penalties for the IEEE 57 bus system.

Hour	Direct cost wind ($/h)	Underestimation penalty wind ($/h)	Overestimation penalty wind ($/h)	Direct cost solar ($/h)	Overestimation penalty solar ($/h)	Underestimation penalty solar ($/h)	Thermal cost ($/h)	Total Fuel cost $/h	Emission (ton/h)
1	46.1838	1.47	0	0	0	0	1740.536	1788.191	1293.992
2	48.3648	0	6.8033	0	0	0	2511.4	2566.569	1078.96
3	57.9700	0	0	0	0	0	2628.349	2686.319	2127.774
4	81.1258	9.9259	0	0	0	0	3403.847	3494.899	2678.613
5	82.6100	10.0000	0	0	0	0	3755.964	3848.574	3111.316
6	116.2755	0	0.5019	1.6319	1.6436	0	3869.333	3989.386	4381.615
7	147.1728	10.6561	0	3.9522	0.7062	0	3936.124	4098.611	4930.788
8	115.4937	0	39.4276	12.2034	0	2.4010	4398.143	4567.669	5763.601
9	123.1992	10.0718	0	13.2550	5.0000	0	5011.244	5162.77	7250.21
10	134.3759	0	5.9909	19.0049	4.2843	0	6326.27	6489.926	6955.339
11	110.0550	5.0000	0	17.4802	0	4.1074	6969.73	7106.373	7982.814
12	69.2974	0	9.7604	17.9019	0	0.4458	6931.242	7028.648	9437.62
13	67.8439	0	14.6312	21.2954	0.0561	0	6939.34	7043.167	7478.188
14	47.4605	6.4061	0	17.5409	0	2.6266	6566.22	6640.254	6391.192
15	81.3985	0.1323	0	15.8464	1.4208	0	4901.461	5000.259	5494.513
16	48.3045	7.6835	0	8.2338	1.4700	0	4966.619	5032.311	3307.451
17	22.0177	0	1.6125	4.6316	6.9462	0	3451.46	3486.668	3965.083
18	26.8600	0	76.8221	1.0960	8.3616	0	4549.185	4662.325	4639.979
19	4.6414	0	2.9465	0.2183	0.4507	0	4404.968	4413.225	7631.993
20	43.6377	0	6.0672	0	0	0	5522.609	5572.314	7766.047
21	86.4600	4.0000	0	0	0	0	4697.664	4788.124	7728.91
22	167.6164	0	7.8553	0	0	0	3665.766	3841.237	4053.173
23	191.4908	0	8.2577	0	0	0	3329.19	3528.939	1495.608
24	310.1845	11.4083	0	0	0	0	1664.826	1986.419	808.8267
							106141.4909	**108823.1756**	**117753.6056**

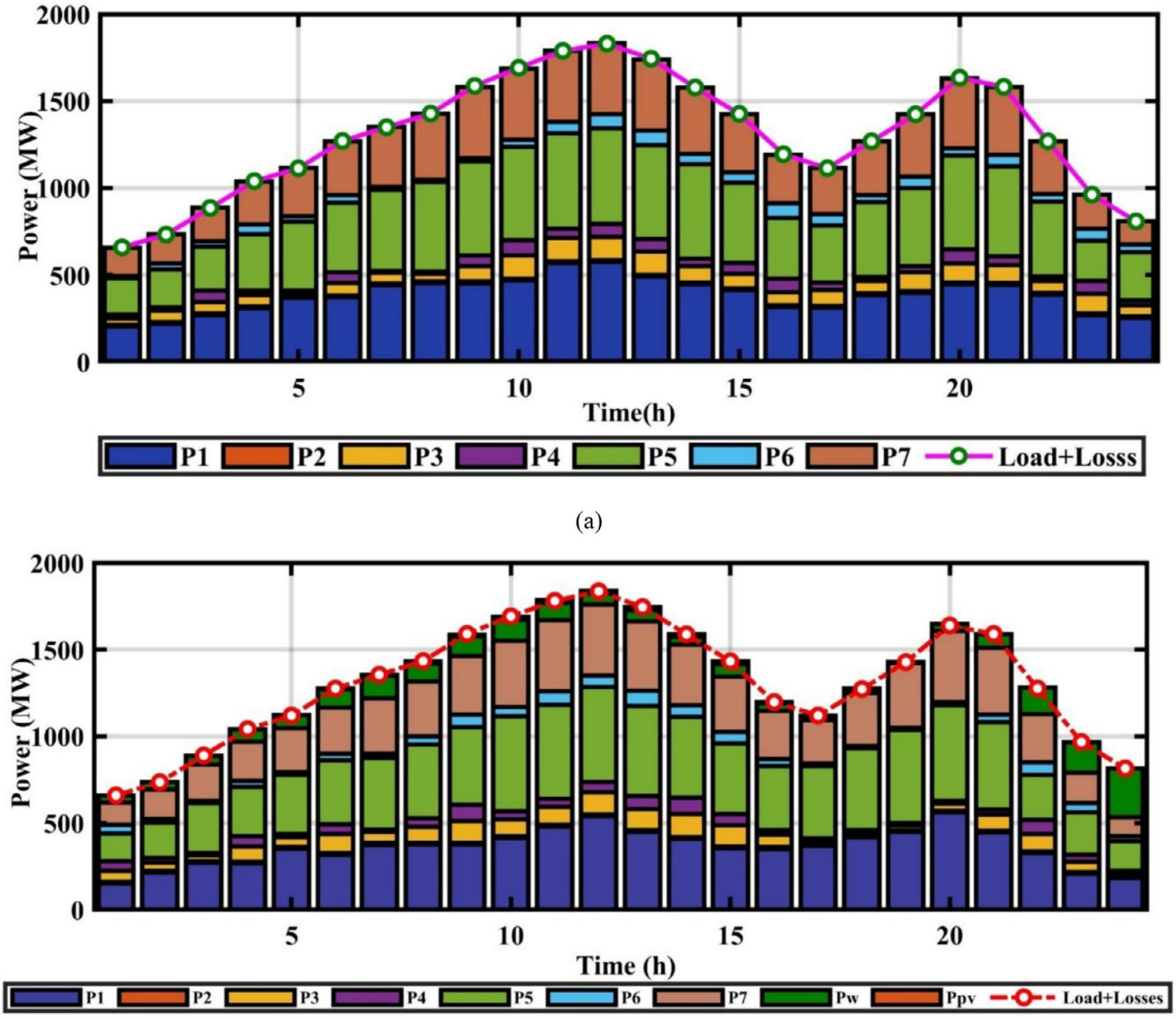

FIGURE 16 | Stacked histogram of dynamic power generation for the IEEE 57 bus system. (a) Without renewables and (b) with renewables.

TABLE 17 | Comparative results for Case IV.

	Situation 1 (without renewable)				
Cost and emission	**PSO**	**BMO**	**AOA**	**DTBO**	**AOASC-DTBO**
Cost ($) ($10^5$)	1.26	1.20	1.25	1.21	1.15
Emission (tonne) (10^5)	1.31	1.39	1.33	1.33	1.30
	Situation 2 (with renewable)				
Cost and emission	**PSO**	**BMO**	**AOA**	**DTBO**	**AOASC-DTBO**
Cost ($) ($10^5$)	1.16	1.11	1.13	1.13	1.08
Emission (tonne) (10^5)	1.21	1.28	1.27	1.25	1.17

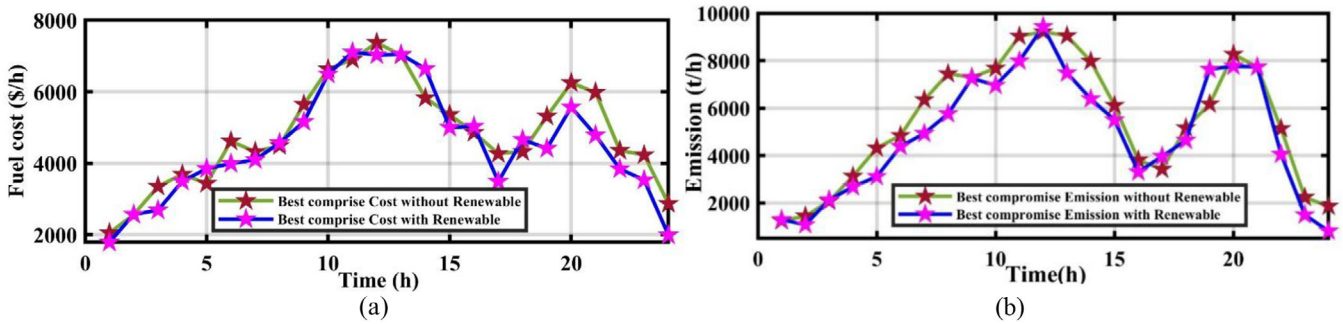

FIGURE 17 | Best compromised with and without renewable for IEEE 57 bus system. (a) Emissions and (b) cost.

cost, which is 8.73% and 4.95% lower than the PSO and DTBO algorithms. Additionally, the emissions for AOASC-DTBO were 6.47% lower than the BMO and 2.25% lower than the DTBO algorithm. In Situation 2, the AOASC-DTBO algorithm achieved a 4.42% reduction in fuel cost compared to the DTBO algorithm, while its emission cost was 6.4% lower than that of the DTBO algorithm. Figure 17 illustrates that utilising wind and PV power results in cost savings of $6908.034 and a reduction in emissions by 13,233.691 tonnes per day.

6 | Discussions

In this study a novel metaheuristic AOASC-DTBO algorithm is proposed to solve the non-convex HDEED problem. While the proposed algorithm has demonstrated remarkable success in solving complex, nonlinear and multi-objective economic dispatch problems, it also possesses several inherent limitations. The key challenges include the stochastic nature demanding multiple independent runs and appropriate parameter tuning. The performance of the AOASC-DTBO algorithm is highly sensitive to the tuning of two key parameters: the sensitivity parameter (α) and the scaling factor (S). Proper tuning of these parameters is essential for achieving better convergence and optimal dispatch results. In this study, the values $\alpha = 2.5$ and $S = 0.05$ were found to yield the best results for both economic dispatch and wind/PV power prediction. These parameter settings provided the most efficient performance in the context of our experiments. The experimental results, as presented in Section 5, demonstrate the superior performance of AOASC-DTBO in terms of better dispatch outcomes.

However, one of the primary drawbacks of the algorithm is its computational time complexity. While this is not an issue in our study, as we are dealing with an offline economic dispatch problem, it remains an important consideration. The hybridisation process improves the algorithm's performance but also increases its time complexity. For instance, the simulation time required by the AOASC-DTBO algorithm to compute the fuel cost for the 40-unit system was 180.475 s, compared to 118.790 s for DTBO, 98.075 s for BMO, 77.218 s for PSO and 46.1203 s for AOA. These simulations were performed on an 11th Gen Intel Core i5 processor with 16 GB RAM, using a population size of 1000 and considering 1000 iterations. Furthermore, the dispatch results are strongly influenced by the accuracy of wind and PV power forecasts. Reliable predictions of photovoltaic (PV) and wind power contribute to reduced reserve requirements, improved grid stability, and lower overall dispatch costs. Conversely, poor forecasting accuracy leads to operational inefficiencies and increased dispatch expenses. The results presented in Sections 5.4 and 5.5 were obtained using forecasting accuracies corresponding to R^2 values of 0.9194 for wind and 0.9696 for PV, as shown in Table 2. With these prediction accuracies, the AOASC-DTBO algorithm achieved a cost reduction of $168,637.9 per day and a decrease in emissions by 27,052.774 tonnes per day in Case III. However, when the analysis was performed using lower forecasting accuracy, the dispatch costs increased, indicating the strong dependence of dispatch performance on renewable power prediction precision.

7 | Conclusion

This paper proposed a novel method to solve the HDEED problem by considering the impact of RES on the fuel cost and pollutant emissions of the power system. The proposed arithmetic optimisation algorithm with a sine cosine assisted driving training-based algorithm (AOASC-DTBO) outperformed other algorithms in terms of reducing the emissions and fuel cost. For a 10-unit system, the AOASC-DTBO algorithm achieved a minimum cost of 2.53e6, which is 12.1% and 2.31% lower than that of the AOA and PSO algorithms, respectively. Additionally, the AOASC-DTBO algorithm attained emissions of 2.97e5, which are 17.51% and 5.71% lower than those of the AOA and DTBO algorithms, respectively. In addition, using data-driven forecasting techniques to predict the wind and PV power allowed for better and more practical optimisation of the generation schedule. Furthermore, the integration of renewable energy into the existing power systems resulted in cost and emission reductions of $168637.9 and 27052.774 tonnes/day, respectively. The results demonstrated the potential cost savings and emission reductions by the AOASC-DTBO algorithm for optimal dispatching of different power generation units.

Nomenclature

Acronyms

ANN	Artificial neural network
AOASC-DTBO	Arithmetic optimiser with sine cosine assisted driving training-based optimisation algorithm
DEED	Dynamic economic emission dispatch
DTBO	Driving training-based optimisation

EED	Economic emission dispatch
ELD	Economic load dispatch
HDEED	Hybrid dynamic economic emission dispatch
MOP	Math optimisation probability
NN	Neural network
NRMSE	Normalised root mean square error
PSO	Particle swarm optimisation
PFs	Pareto fronts
RBFNN	Radial basis function neural network
BCSs	Best compromise solutions
RES	Renewable energy sources
R^2	Coefficient of determination

Variables

a_i, b_i, c_i	Cost coefficients
d_i, e_i	Valve point coefficients
$\alpha_i, \beta_i, \gamma, \zeta_i, \delta_i$	Emission coefficients
E_c	Emission cost
F_c	Fuel cost
F_O	Overestimation reserve cost
$F_{O,wk}$	Overestimation reserve cost for wind generation
F_U	Underestimation penalty
$F_{U,wk}$	Underestimation penalty for wind generation
F_{wk}	Direct cost for wind power generation
k_{Op}	Overestimation cost coefficient
k_{up}	Underestimation penalty coefficient
it	Iteration
Max_it	Maximum iteration
N	Number of selected neurons
NG	Number of thermal units
NS	Number of solar units
NW	Number of wind units
S	Sensitivity parameter
t	Time horizon

Author Contributions

Muhammad Kamran Khan: conceptualisation, data curation, formal analysis, investigation, methodology, writing – original draft, writing – review and editing. **Muhammad Ammar Khan**: methodology, software, writing – original draft, writing – review and editing. **Kimmo Kauhaniemi**: conceptualisation, formal analysis, funding acquisition, supervision, validation, writing – review and editing. **Muhammad Hamza Zafar**: conceptualisation, investigation, methodology, software. **Saad Rashid**: formal analysis, methodology, writing – original draft.

Acknowledgements

This work was carried out under projects titled Smart Grid 2.0, with financial support provided by Business Finland under Grant #1386/31/2022.

Open access publishing facilitated by Vaasan yliopisto, as part of the Wiley - FinELib agreement.

Conflicts of Interest

The authors declare no conflicts of interest.

Data Availability Statement

Data will be made available on request.

References

1. Z.-F. Liu, L.-L. Li, Y.-W. Liu, J.-Q. Liu, H.-Y. Li, and Q. Shen, "Dynamic Economic Emission Dispatch Considering Renewable Energy Generation: A Novel Multi-Objective Optimization Approach," *Energy* 235 (2021): 121407, https://doi.org/10.1016/j.energy.2021.121407.

2. M. Q. Wang, H. B. Gooi, S. X. Chen, and S. Lu, "A Mixed Integer Quadratic Programming for Dynamic Economic Dispatch With Valve Point Effect," *IEEE Transactions on Power Systems* 29, no. 5 (2014): 2097–2106, https://doi.org/10.1109/TPWRS.2014.2306933.

3. J. P. Zhan, Q. H. Wu, C. X. Guo, and X. X. Zhou, "Fast λ-Iteration Method for Economic Dispatch With Prohibited Operating Zones," *IEEE Transactions on Power Systems* 29, no. 2 (2014): 990–991, https://doi.org/10.1109/TPWRS.2013.2287995.

4. W.-M. Lin and S.-J. Chen, "Bid-Based Dynamic Economic Dispatch With an Efficient Interior Point Algorithm," *International Journal of Electrical Power & Energy Systems* 24, no. 1 (2002): 51–57, https://doi.org/10.1016/S0142-0615(01)00007-2.

5. S. Janefar, P. Chowdhury, R. Yeassin, M. Hasan, and N.-U.-R. Chowdhury, "Comparative Performance Evaluation of Economic Load Dispatch Using Metaheuristic Techniques: A Practical Case Study for Bangladesh," *Results in Engineering* 26 (2025): 104720, https://doi.org/10.1016/j.rineng.2025.104720.

6. N. A. Alawad, B. H. Abed-Alguni, and M. El-Ibini, "Hybrid Snake Optimizer Algorithm for Solving Economic Load Dispatch Problem With Valve Point Effect," *The Journal of Supercomputing* 80, no. 13 (2024): 19274–19323, https://doi.org/10.1007/s11227-024-06207-5.

7. W.-K. Hao, J.-S. Wang, X.-D. Li, M. Wang, and M. Zhang, "Arithmetic Optimization Algorithm Based on Elementary Function Disturbance for Solving Economic Load Dispatch Problem in Power System," *Applied Intelligence* 52, no. 10 (2022): 11846–11872, https://doi.org/10.1007/s10489-021-03125-4.

8. M. A. Al-Betar, M. A. Awadallah, R. A. Zitar, and K. Assaleh, "Economic Load Dispatch Using Memetic Sine Cosine Algorithm," *Journal of Ambient Intelligence and Humanized Computing* 14 (2022): 11685–11713, https://doi.org/10.1007/s12652-022-03731-1.

9. T. Singh, "Chaotic Slime Mould Algorithm for Economic Load Dispatch Problems," *Applied Intelligence* 52, no. 13 (2022): 15325–15344, https://doi.org/10.1007/s10489-022-03179-y.

10. A. Srivastava and D. K. Das, "An Adaptive Chaotic Class Topper Optimization Technique to Solve Economic Load Dispatch and Emission Economic Dispatch Problem in Power System," *Soft Computing* 26, no. 6 (2022): 2913–2934, https://doi.org/10.1007/s00500-021-06644-x.

11. Y. Wang, X. Yu, and W. Zhang, "An Improved Reinforcement Learning-Based Differential Evolution Algorithm for Combined Economic and Emission Dispatch Problems," *Engineering Applications of Artificial Intelligence* 140 (2025): 109709, https://doi.org/10.1016/j.engappai.2024.109709.

12. Y.-X. Li, J.-S. Wang, X.-Y. Guan, X.-T. Wang, X. Liu, and S.-B. Zhang, "Arithmetic Optimization Algorithm With Three-Dimensional Chaotic Mapping in Spherical Coordinate System for Combined Economic Emission Dispatch Problem," *Applied Energy* 380 (2025): 124953, https://doi.org/10.1016/j.apenergy.2024.124953.

13. K. He, Y. Zhang, Y. Wang, and R. Zhou, "Solving Power System Economic Emission Dispatch Problem Under Complex Constraints via Dimension Differential Learn Butterfly Optimization Algorithm With FDC-Based," *Computers & Industrial Engineering* 197 (2024): 110568, https://doi.org/10.1016/j.cie.2024.110568.

14. M. H. Hassan, S. Kamel, F. Jurado, and U. Desideri, "Global Optimization of Economic Load Dispatch in Large Scale Power Systems Using an Enhanced Social Network Search Algorithm," *International Journal of Electrical Power & Energy Systems* 156 (2024): 109719, https://doi.org/10.1016/j.ijepes.2023.109719.

15. A. Arkwazee and R. Abttan, "Enhanced Zebra Optimization Algorithm for Sustainable Combined Economic and Emission Dispatch in Power Systems," *Array* 27: 100484.

16. R. Arul, S. Velusami, and G. Ravi, "A New Algorithm for Combined Dynamic Economic Emission Dispatch With Security Constraints," *Energy* 79 (2015): 496–511, https://doi.org/10.1016/j.energy.2014.11.037.

17. L.-L. Li, Z.-F. Liu, M.-L. Tseng, S.-J. Zheng, and M. K. Lim, "Improved Tunicate Swarm Algorithm: Solving the Dynamic Economic Emission Dispatch Problems," *Applied Soft Computing* 108 (2021): 107504, https://doi.org/10.1016/j.asoc.2021.107504.

18. V. K. Jadoun, N. Gupta, K. R. Niazi, and A. Swarnkar, "Modulated Particle Swarm Optimization for Economic Emission Dispatch," *International Journal of Electrical Power & Energy Systems* 73 (2015): 80–88, https://doi.org/10.1016/j.ijepes.2015.04.004.

19. M. H. Hassan, S. Kamel, L. Abualigah, and A. Eid, "Development and Application of Slime Mould Algorithm for Optimal Economic Emission Dispatch," *Expert Systems With Applications* 182 (2021): 115205, https://doi.org/10.1016/j.eswa.2021.115205.

20. M. F. Zaman, S. M. Elsayed, T. Ray, and R. A. Sarker, "Evolutionary Algorithms for Dynamic Economic Dispatch Problems," *IEEE Transactions on Power Systems* 31, no. 2 (2016): 1486–1495, https://doi.org/10.1109/TPWRS.2015.2428714.

21. M. H. Hassan, S. Kamel, S. Q. Salih, T. Khurshaid, and M. Ebeed, "Developing Chaotic Artificial Ecosystem-Based Optimization Algorithm for Combined Economic Emission Dispatch," *IEEE Access* 9 (2021): 51146–51165, https://doi.org/10.1109/ACCESS.2021.3066914.

22. V. Ravikumar Pandi and B. K. Panigrahi, "Dynamic Economic Load Dispatch Using Hybrid Swarm Intelligence Based Harmony Search Algorithm," *Expert Systems With Applications* 38, no. 7 (2011): 8509–8514, https://doi.org/10.1016/j.eswa.2011.01.050.

23. B. Dey, F. P. García Márquez, P. Kumar Panigrahi, and B. Bhattacharyya, "A Novel Metaheuristic Approach to Scale the Economic Impact of Grid Participation on a Microgrid System," *Sustainable Energy Technologies and Assessments* 53 (2022): 102417, https://doi.org/10.1016/j.seta.2022.102417.

24. N. Pandit, A. Tripathi, S. Tapaswi, and M. Pandit, "An Improved Bacterial Foraging Algorithm for Combined Static/Dynamic Environmental Economic Dispatch," *Applied Soft Computing* 12, no. 11 (2012): 3500–3513, https://doi.org/10.1016/j.asoc.2012.06.011.

25. S. Qian, H. He, H. Wu, P. Fournier-Viger, H. Li, and S. Huang, "A Hybrid Constrained Multi-Objective Algorithm for Dynamic Economic Emission Dispatch," *International Journal of Electrical Power & Energy Systems* 169 (2025): 110711, https://doi.org/10.1016/j.ijepes.2025.110711.

26. S. B. Pandya, K. Kalita, P. Jangir, et al., "Multi-Objective RIME Algorithm-Based Techno Economic Analysis for Security Constraints Load Dispatch and Power Flow Including Uncertainties Model of Hybrid Power Systems," *Energy Reports* 11 (2024): 4423–4451, https://doi.org/10.1016/j.egyr.2024.04.016.

27. S. Qian, H. Wu, and G. Xu, "An Improved Particle Swarm Optimization With Clone Selection Principle for Dynamic Economic Emission Dispatch," *Soft Computing* 24, no. 20 (2020): 15249–15271, https://doi.org/10.1007/s00500-020-04861-4.

28. L.-L. Li, Q. Shen, M.-L. Tseng, and S. Luo, "Power System Hybrid Dynamic Economic Emission Dispatch With Wind Energy Based on Improved Sailfish Algorithm," *Journal of Cleaner Production* 316 (2021): 128318, https://doi.org/10.1016/j.jclepro.2021.128318.

29. I. Marouani, T. Guesmi, H. Hadj Abdallah, et al., "Combined Economic Emission Dispatch With and Without Consideration of PV and Wind Energy by Using Various Optimization Techniques: A Review," *Energies* 15, no. 12 (2022): 4472, https://www.mdpi.com/1996-1073/15/12/4472.

30. W. Wei, H. Ouyang, W. Wu, S. Li, and D. Zou, "A Behavior-Selection Based Rao Algorithm and Its Applications to Power System Economic Load Dispatch Problems," *Applied Intelligence* 52, no. 10 (2022): 11966–11999, https://doi.org/10.1007/s10489-021-02849-7.

31. B. Qiao, Z. Feng, Z. Zhu, et al., "Multi-Objective Dynamic Economic Emission Dispatch Considering the Risk of Wind Power-Electric Vehicle Interaction Using Teaching-Learning-Based Optimization Algorithm," *Swarm and Evolutionary Computation* 98 (2025): 102096, https://doi.org/10.1016/j.swevo.2025.102096.

32. G. Xiong, Q. Liu, Y. Wang, and X. Fu, "Power System Economic Emission Dispatch Considering Uncertainties of Wind, Solar, and Small Runoff Hydropower via a Hybrid Multi-Objective Optimization Algorithm," *Expert Systems With Applications* 278 (2025): 127375, https://doi.org/10.1016/j.eswa.2025.127375.

33. W.-K. Hao, J. S. Wang, X. D. Li, et al., "Multi-Objective Arithmetic Optimization Algorithm With Random Searching Strategies to Solve Combined Economic Emission Dispatch Problem," *Computers & Industrial Engineering* 195 (2024): 110434, https://doi.org/10.1016/j.cie.2024.110434.

34. M. I. K. Khalil, I. U. Rahman, M. Zakarya, et al., "A Multi-Objective Optimisation Approach With Improved Pareto-Optimal Solutions to Enhance Economic and Environmental Dispatch in Power Systems," *Scientific Reports* 14, no. 1 (2024): 13418, https://doi.org/10.1038/s41598-024-62904-4.

35. G. Xiong, M. Shuai, and X. Hu, "Combined Heat and Power Economic Emission Dispatch Using Improved Bare-Bone Multi-Objective Particle Swarm Optimization," *Energy* 244 (2022): 123108, https://doi.org/10.1016/j.energy.2022.123108.

36. A. Sundaram, "Multiobjective Multi Verse Optimization Algorithm to Solve Dynamic Economic Emission Dispatch Problem With Transmission Loss Prediction by an Artificial Neural Network," *Applied Soft Computing* 124 (2022): 109021, https://doi.org/10.1016/j.asoc.2022.109021.

37. H. Nourianfar and H. Abdi, "Solving the Multi-Objective Economic Emission Dispatch Problems Using Fast Non-Dominated Sorting TVAC-PSO Combined With EMA," *Applied Soft Computing* 85 (2019): 105770, https://doi.org/10.1016/j.asoc.2019.105770.

38. M. Modiri-Delshad and N. A. Rahim, "Multi-Objective Backtracking Search Algorithm for Economic Emission Dispatch Problem," *Applied Soft Computing* 40 (2016): 479–494, https://doi.org/10.1016/j.asoc.2015.11.020.

39. M. H. Hassan, D. Yousri, S. Kamel, and C. Rahmann, "A Modified Marine Predators Algorithm for Solving Single- and Multi-Objective Combined Economic Emission Dispatch Problems," *Computers & Industrial Engineering* 164 (2022): 107906, https://doi.org/10.1016/j.cie.2021.107906.

40. W. Lai, X. Zheng, Q. Song, F. Hu, Q. Tao, and H. Chen, "Multi-Objective Membrane Search Algorithm: A New Solution for Economic Emission Dispatch," *Applied Energy* 326 (2022): 119969, https://doi.org/10.1016/j.apenergy.2022.119969.

41. N. Ghorbani, E. Babaei, and F. Sadikoglu, "Exchange Market Algorithm for Multi-Objective Economic Emission Dispatch and Reliability," *Procedia Computer Science* 120 (2017): 633–640, https://doi.org/10.1016/j.procs.2017.11.289.

42. W. Sheng, R. Li, T. Yan, M.-L. Tseng, J. Lou, and L. Li, "A Hybrid Dynamic Economics Emissions Dispatch Model: Distributed Renewable Power Systems Based on Improved COOT Optimization Algorithm," *Renewable Energy* 204 (2023): 493–506, https://doi.org/10.1016/j.renene.2023.01.010.

43. G. Wang, Y. Zha, T. Wu, J. Qiu, J.-C. Peng, and G. Xu, "Cross Entropy Optimization Based on Decomposition for Multi-Objective Economic Emission Dispatch Considering Renewable Energy Generation

Uncertainties," *Energy* 193 (2020): 116790, https://doi.org/10.1016/j.energy.2019.116790.

44. R. Dong, L. Sun, Z. Cai, A. A. Heidari, L. Liu, and H. Chen, "An Advanced Kernel Search Optimization for Dynamic Economic Emission Dispatch With New Energy Sources," *International Journal of Electrical Power & Energy Systems* 160 (2024): 110085, https://doi.org/10.1016/j.ijepes.2024.110085.

45. D. Verma, J. Soni, and K. Bhattacharjee, "A Novel Artificial Electric Field Strategy for Economic Load Dispatch Problem With Renewable Penetration," *Evolutionary Intelligence* 17, no. 5 (2024): 3593–3608, https://doi.org/10.1007/s12065-024-00946-3.

46. L.-L. Li, J.-L. Lou, M.-L. Tseng, M. K. Lim, and R. R. Tan, "A Hybrid Dynamic Economic Environmental Dispatch Model for Balancing Operating Costs and Pollutant Emissions in Renewable Energy: A Novel Improved Mayfly Algorithm," *Expert Systems With Applications* 203 (2022): 117411, https://doi.org/10.1016/j.eswa.2022.117411.

47. V. K. Jadoun, V. C. Pandey, N. Gupta, K. R. Niazi, and A. Swarnkar, "Integration of Renewable Energy Sources in Dynamic Economic Load Dispatch Problem Using an Improved Fireworks Algorithm," *IET Renewable Power Generation* 12, no. 9 (2018): 1004–1011, https://doi.org/10.1049/iet-rpg.2017.0744.

48. M. Dehghani, E. Trojovská, and P. Trojovský, "A New Human-Based Metaheuristic Algorithm for Solving Optimization Problems on the Base of Simulation of Driving Training Process," *Scientific Reports* 12, no. 1 (2022): 9924, https://doi.org/10.1038/s41598-022-14225-7.

49. S. Mirjalili, "SCA: A Sine Cosine Algorithm for Solving Optimization Problems," *Knowledge-Based Systems* 96 (2016): 120–133, https://doi.org/10.1016/j.knosys.2015.12.022.

50. L. Abualigah, A. Diabat, S. Mirjalili, M. A. Elaziz, and A. H. Gandomi, "The Arithmetic Optimization Algorithm," *Computer Methods in Applied Mechanics and Engineering* 376 (2021): 113609, https://doi.org/10.1016/j.cma.2020.113609.

51. S. Mirjalili, S. M. Mirjalili, and A. Lewis, "Grey Wolf Optimizer," *Advances in Engineering Software* 69 (2014): 46–61, https://doi.org/10.1016/j.advengsoft.2013.12.007.

52. M. K. Sayadi, A. Hafezalkotob, and S. G. J. Naini, "Firefly-Inspired Algorithm for Discrete Optimization Problems: An Application to Manufacturing Cell Formation," *Journal of Manufacturing Systems* 32, no. 1 (2013): 78–84, https://doi.org/10.1016/j.jmsy.2012.06.004.

53. J. Pierezan and L. D. S. Coelho, "Coyote Optimization Algorithm: A New Metaheuristic for Global Optimization Problems," in *2018 IEEE Congress on Evolutionary Computation (CEC)* (IEEE, 2018), 1–8, https://doi.org/10.1109/CEC.2018.8477769.

54. M. Hamza Zafar, N. Mujeeb Khan, M. Mansoor, A. Feroz Mirza, S. Kumayl Raza Moosavi, and F. Sanfilippo, "Adaptive ML-Based Technique for Renewable Energy System Power Forecasting in Hybrid PV-Wind Farms Power Conversion Systems," *Energy Conversion and Management* 258 (2022): 115564, https://doi.org/10.1016/j.enconman.2022.115564.

55. C. Ge, J. Yan, H. Zhang, Y. Li, H. Wang, and Y. Liu, "Joint Short-Term Power Forecasting of Hydro-Wind-Photovoltaic Considering Spatiotemporal Delay of Weather Processes," *Renewable Energy* 237 (2024): 121679, https://doi.org/10.1016/j.renene.2024.121679.

56. M. K. Khan, M. H. Zafar, S. Rashid, M. Mansoor, S. K. R. Moosavi, and F. Sanfilippo, "Improved Reptile Search Optimization Algorithm: Application on Regression and Classification Problems," *Applied Sciences* 13, no. 2 (2023): 945, https://www.mdpi.com/2076-3417/13/2/945.

57. B. Erisen, "Wind Turbine SCADA Dataset," Kaggle, 2018. [Online]. Available: https://www.kaggle.com/datasets/berkerisen/wind-turbine-scada-dataset.

58. A. Kannal, "Solar Power Generation Data," Kaggle. [Online]. Available: https://www.kaggle.com/datasets/anikannal/solar-power-generation-data.

59. D. Zou, S. Li, Z. Li, and X. Kong, "A New Global Particle Swarm Optimization for the Economic Emission Dispatch With or Without Transmission Losses," *Energy Conversion and Management* 139 (2017): 45–70, https://doi.org/10.1016/j.enconman.2017.02.035.

60. M. Singh and J. Dhillon, "Multiobjective Thermal Power Dispatch Using Opposition-Based Greedy Heuristic Search," *International Journal of Electrical Power & Energy Systems* 82 (2016): 339–353, https://doi.org/10.1016/j.ijepes.2016.03.016.

61. M. Ghasemi, E. Akbari, A. Rahimnejad, S. E. Razavi, S. Ghavidel, and L. Li, "Phasor Particle Swarm Optimization: A Simple and Efficient Variant of PSO," *Soft Computing* 23, no. 19 (2019): 9701–9718, https://doi.org/10.1007/s00500-018-3536-8.

62. K. Mason, J. Duggan, and E. Howley, "A Multi-Objective Neural Network Trained With Differential Evolution for Dynamic Economic Emission Dispatch," *International Journal of Electrical Power & Energy Systems* 100 (2018): 201–221, https://doi.org/10.1016/j.ijepes.2018.02.021.

63. G. Mohy-ud-din, "Hybrid Dynamic Economic Emission Dispatch of Thermal, Wind, and Photovoltaic Power Using the Hybrid Backtracking Search Algorithm With Sequential Quadratic Programming," *Journal of Renewable and Sustainable Energy* 9, no. 1 (2017): 015502, https://doi.org/10.1063/1.4973715.